processes

MDPI

*Review*

# A Review of the Hydraulic Fracturing in Ductile Reservoirs: Theory, Simulation, and Experiment

**Dawei Zhu [1], Guofeng Han [2,3,*], Honglan Zou [1], Mingyue Cui [1], Chong Liang [1] and Fei Yao [1]**

[1] Research Institute of Petroleum Exploration and Development, PetroChina, Beijing 100083, China
[2] Institute of Mechanics, Chinese Academy of Sciences, Beijing 100190, China
[3] School of Engineering Science, University of Chinese Academy of Sciences, Beijing 100049, China
* Correspondence: hanguofeng@imech.ac.cn

**Abstract:** The bottom-hole pressure of hydraulic fracturing in ductile reservoirs is much higher than that of the hydraulic fracturing simulation, and the fracture toughness inferred from the field data is 1–3 orders of magnitude higher than that measured in the laboratory. The rock apparent fracture toughness increases with the increase in the confining pressure. Excluding the influence of the fluid viscosity and the fluid lag on the apparent fracture toughness, the fracture process zone (FPZ) at the fracture tip can explain the orders of magnitude of difference in the apparent fracture toughness between the laboratory and the field. The fracture tip is passivated by plastic deformation, forming a wide and short hydraulic fracture. However, the size of the FPZ obtained in the laboratory is in the order of centimeters to decimeters, while an FPZ of 10 m magnitude is speculated in the field. The FPZ size is affected by the rock property, grain size, pore fluid, temperature, loading rate, and loading configuration. It is found that the FPZ has a size effect that tends to disappear when the rock specimen size reaches the scale of meters. However, this cannot fully explain the experience of hydraulic fracturing practice. The hydraulic fracturing behavior is also affected by the relation between the fracture toughness and the fracture length. The fracture behavior of type II and mixed type for the ductile rock is poorly understood. At present, the apparent fracture toughness model and the cohesive zone model (CZM) are the most suitable criteria for the fracture propagation in ductile reservoirs, but they cannot fully characterize the influence of the rock plastic deformation on the hydraulic fracturing. The elastic-plastic constitutive model needs to be used to characterize the stress–strain behavior in the hydraulic fracturing simulation, and the fracture propagation criteria suitable for ductile reservoirs also need to be developed.

**Keywords:** hydraulic fracturing; ductile rock; plastic deformation; fracture toughness; fracture process zone

check for updates

**Citation:** Zhu, D.; Han, G.; Zou, H.; Cui, M.; Liang, C.; Yao, F. A Review of the Hydraulic Fracturing in Ductile Reservoirs: Theory, Simulation, and Experiment. *Processes* **2022**, *10*, 2022. https://doi.org/10.3390/pr10102022

Academic Editors: Xiang Sun, Yizhao Wan and Lunxiang Zhang

Received: 4 September 2022
Accepted: 27 September 2022
Published: 7 October 2022



## 1. Introduction

With the depletion of conventional oil and gas resources, low-permeability oil and gas resources have become the main force of oil and gas exploration and development, especially the development, in recent decades, of unconventional shale oil and gas, and tight oil and gas [1–3]. The permeability of these reservoirs is very low, which requires stimulations to improve production. Even the industrial oil and gas flows can be obtained only after successful stimulations for some reservoirs [4–7]. Hydraulic fracturing is the most commonly used reservoir stimulation method. To optimize and design the hydraulic fracturing process, the fracturing procedure needs to be simulated and analyzed [8]. It involves the initiation and propagation of rock fractures. Generally, the fracture propagation criterion of linear elastic fracture mechanics is used by commercial hydraulic fracturing simulation software. In the past 60 years, great success has been achieved for the hydraulic fracturing simulation in hard rocks with linear elastic fracture mechanics. However, some reservoir rocks have strong ductility, such as clay sandstone, weakly consolidated sandstone,

clay-rich ductile shale, soft carbonate reservoir, high-temperature reservoir, and coal rock, etc. [9–11]. When they are fractured, a large range of plastic deformation occurs. For these types of reservoirs, current commercial modeling software often fails to produce the right results. The injection pressure simulated by the hydraulic fracturing software with the fracture toughness tested in the laboratory is lower than the actual injection pressure. The fracture propagation net pressure in the field is 50%–100% higher than the results of the software simulation [12]. For poorly consolidated reservoirs, the results are more different [13]. In order to obtain the appropriate injection pressure, the fracture toughness used by designers in the hydraulic fracturing simulation is generally more than one order of magnitude larger than the results tested in the laboratory. The main reason for these problems is that the linear elastic fracture mechanics do not consider the effect of the rock plastic deformation on the crack propagation.

Massive microcracks are generated at the tip during fracture propagation, forming an FPZ and presenting plastic deformation. Over the past 30 years, the effect of rock plastic deformation on the crack propagation has been studied extensively [14–18]. The width of the hydraulic fractures is increased, its length is decreased, and the injection pressure is elevated by the rock plastic deformation [19–23]. The rock permeability near the fracture wall is also changed by it [24]. The FPZ at the fracture tip makes its propagation law different from the linear elastic fracture criterion, which poses a challenge to the accurate hydraulic fracturing simulation of ductile reservoirs. In this paper, the phenomenon of the rock fracture in the laboratory experiments and in the field, the FPZ of rocks, the fracture propagation criteria of ductile rocks, and the hydraulic fracturing simulation considering the rock plastic deformation are reviewed. Finally, the present research status is summarized and the future research is prospected.

## 2. Phenomenon and Explanation

As early as the 1980s, hydraulic fracturing practices showed that the fracture initiation in ductile shale is more difficult than in brittle rocks [25]. The net pressure of fracture propagation in ductile reservoirs is much larger than the prediction of the linear elastic fracture mechanics [26–30]. The fracture toughness inferred from a large number of field tests is 1–2 orders of magnitude greater than that measured in the laboratory [11,27,31–33]. The formation of dikes is a natural hydraulic fracturing process driven by magma [34]. Studies have shown that in this process, an apparent fracture toughness of up to 100–4000 MPa $\cdot \sqrt{\mathrm{m}}$ is often required to obtain a fracture size that is coordinated with field observations [35–40]. This is 2–3 orders of magnitude higher than laboratory measurements [41,42]. Many explanations have been proposed for the vast difference between the field experiences and the laboratory result. These include much higher than expected frictional resistances in perforated Wells, very large near-wellbore bending pressure lost [43,44], increased fracturing fluid viscosity due to filtration and proppant, turbulence in fractures, roughness of the fracture surface [45,46], and restrictions on fracture opening caused by natural joints and fractures in hydraulic fracturing. These factors are related to frictional resistances caused by fluid viscosity. Uneven pressure distribution is caused by these frictions in the fracture. To eliminate the influence of the friction resistance, the instantaneous shut-in pressure was proposed by Shlyapobersky et al. [33] to calculate the net pressure of the fracture propagation (Figure 1). The apparent fracture toughness obtained after eliminating the friction resistance is still much higher than that obtained using laboratory tests. In the hydraulic fracturing practice, not only must the resistance of fracture propagation caused by the rock material property be overcome, but a lot of energy is also consumed to overcome the resistance caused by other external factors. The apparent fracture toughness is often used to represent the resistance to the fracture propagation, including the intrinsic property of the rock material and that caused by other external factors.

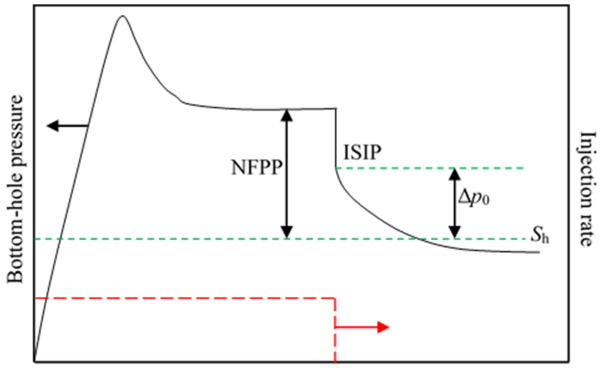


**Figure 1.** The schematic of the pressure response for the hydraulic fracture treatment. (NFPP—net fracture propagation pressure; ISIP—instantaneous shut-in pressure; $S_h$—closing stress; $\Delta p_0$—net fracture pressure.).

It was found in the experiment that the propagating fracture is not completely filled by the fracturing fluid (Figure 2). The fracturing fluid flow lags the fracture propagation rate, and there is a fluid lag zone behind the fracture tip [47–49]. The length of the fluid lag zone increases with the increase in the fluid viscosity [50,51]. The presence of the fluid lag zone is equivalent to a reduction in the driving force of the fracture propagation, which increases the rock apparent fracture toughness. The longer the fluid lag zone, the greater the increase in the apparent fracture toughness. During the fracture initiation, a mass of microcracks is generated near the front of the fracture tip, which means that the rock is yielded at the fracture tip. This part rock is no longer elastic but is in plastic deformation [52]. This area is known as the FPZ [53–56]. After the fracture tip propagates away, this yield zone becomes the fracture wall. The rock may dilate after yield. Cleary et al. [20,57] believed that the rock dilation would reduce the fracture opening and limit the flow of the fracturing fluid to the fracture tip. Therefore, the fluid lag zone is increased, and a higher-pressure drop is formed. Thus, the rock-apparent fracture toughness is increased. However, the simulation study of Thiercelin and Papanastasiou [11,21] showed that the fracture opening, considering the plastic deformation, is larger, and the fracture passivated by the plasticity of the fracture tip and the fracture opening is increased. Thus, the fluid lag zone would be shortened, and the fracture toughness would be reduced. These studies are aimed at type I fractures. Much attention has been attracted by the development of shale gas in the last decade with the shear dilation of type II fractures. It is believed that the permeability is increased by the fracture surface roughness after the flowback of the fracturing fluid in unconventional reservoirs, even if there is no proppant in the hydraulic fracture [58–60]. The experiment of Feng and Sarmadivaleh [61] showed that the shear dilation of ductile rocks is more remarkable, and the fracture propagation path is more tortuous. Therefore, the increase in permeability may be more pronounced. It is important to note that the fracture propagation is slow during the hydraulic fracturing in the field and the presence of the fluid lag is questionable in the field.

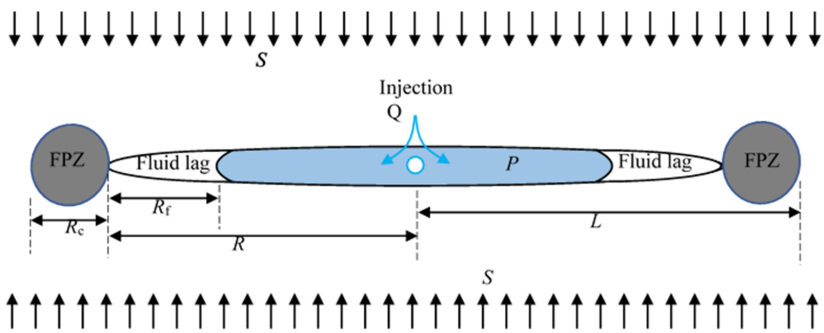


**Figure 2.** The schematic of the Fluid lag zone and FPZ in hydraulic fracturing.

When the rock fracture toughness is evaluated by the hydraulic fracturing, it is usually assumed that the pressure in the fracture is uniform [62]. In fact, the pressure distribution in the fracture is not uniform, due to the fluid viscosity and the fluid lag zone. Many researchers have pointed out that the fracture initiation pressure is inconsistent with the peak bottom-hole pressure due to the compliance of the injection system. The peak pressure is not the fracture initiation pressure. After this moment, the fracture continues to propagate stably for a period of time. The difference between the fracture initiation pressure and the peak bottom-hole pressure is increased by the compliance of the injection system [63–65]. Their difference increases with the compliance of the injection system. In addition, the difference increases with the increase in the fluid viscosity and the confining pressure. These factors make the analysis method proposed by Abou-Sayed inapplicable for determining the fracture toughness. Therefore, Gao et al. [66,67] believe that the increase in the apparent fracture toughness and the fracture pressure with the confining pressure is a hydraulic property. In fact, their model does not consider the FPZ, which is the reason for why their simulated peak pressures are generally lower than experimental ones.

In addition to these reasons, it is believed that a group of parallel multiple fractures rather than a single fracture is produced in the hydraulic fracturing [68–72]. This increases the energy dissipation in the fracture propagation, and thus, increases the apparent fracture toughness. However, the dominant fracture inhibits the propagation of other fractures, and there is no simultaneous propagation of multiple fractures after a distance of propagation in field practices [33]. Therefore, this interpretation is not realistic. In recent decades, the technology of the volume stimulation for improving reservoir productivity has been greatly developed. To achieve an excellent fracturing effect, multiple fractures need to propagate synchronously. It makes this view worthy of further studies.

It has been proven via extensive experiments that the rock fracture toughness increases with an increase in the confining pressure [73–87]. This is shown in Figure 3. The hydraulic fracturing in the field also shows that the rock apparent fracture toughness increases with the increase in the in situ stress. Because there is no fluid involved in the experiment, none of the above-mentioned fluid-related explanations can explain this phenomenon. There are plenty of microcracks in the FPZ, which changes the mechanical properties of the rock [88], and makes it no longer elastic. Additional energy dissipation is added by the confining pressure acting on this zone when a new fracture surface is formed. Therefore, the rock apparent fracture toughness is increased. This is confirmed by the numerical simulation of Hashida et al. [89] and Papanastasiou [12]. The simulation of Papanastasiou [12] shows that an order of magnitude of the fracture toughness can be increased by considering the plastic zone at the crack tip. Rubin [90] and Yue et al. [91] established a rock apparent fracture toughness model, considering the FPZ. It can explain the phenomenon that the rock apparent fracture toughness increases with the increase in the normal stress acting on the fracture surface. It is also found that there is a size effect on the rock apparent fracture toughness. Experiments and simulation studies show that the apparent fracture toughness is affected by the size of the test specimen. With the increase in the test specimen size, the apparent fracture toughness increases [92–96]. The relationship between the nominal tensile strength and the test specimen size meets Bazant's scaling law [94]. The apparent fracture toughness is also affected by the specimen geometry [97–101]. Ayatollahi and Akbardoost [93] explained the influence of the specimen geometry and size on the rock apparent fracture toughness by considering the FPZ.

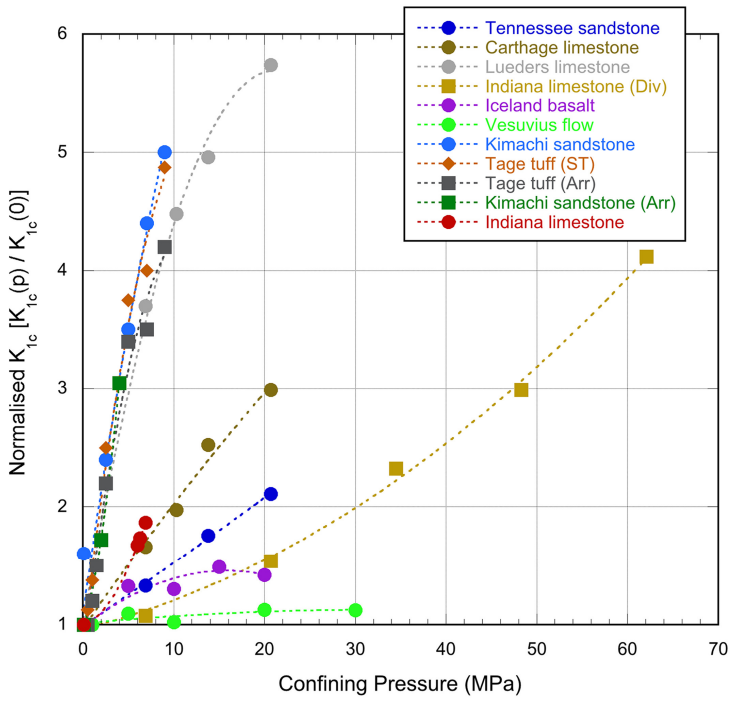


**Figure 3.** The influence of confining pressure on the normalized $K_{Ic}$ for rocks. ($K_{Ic}$ (0): the $K_{Ic}$ measured at ambient pressure). Reprinted with permission from Ref. [78]. Copyright 2020, John Wiley and Sons.

Due to the huge difference between the rock fracture toughness tested in the laboratory and that inferred by the field fracturing, the mini-frac test is generally carried out before formal fracturing in engineering. The fracture toughness obtained from the mini-frac test is used as the parameter for the hydraulic fracturing simulation. However, the size effect of the rock apparent fracture toughness is not only reflected in the difference between the laboratory scale and the field scale. Some studies show that the rock apparent fracture toughness increases with the increase in the fracture length [101–104]. The tests of Hashida et al. [105] on granite specimens from several millimeters to 20 cm show that the rock fracture toughness increases exponentially with the power of the fracture radius. Weisinger et al. [106] found that the fracture toughness of Nevada tuff increases slightly with the increase in the fracture length ranging over 30–70 mm. Scholtz et al. [107–109] speculates that there is a proportional relation between the fracture toughness and the square root of the fracture length, based on the linear relation between the length and the displacement of the dyke. This phenomenon is not unique to the rock fracture toughness. Classical fracture mechanics mainly studies metal materials. For non-ideal brittle materials, the fracture toughness is expressed as a curve of the fracture propagation resistance with the increase in the fracture length. The fracture propagation resistance increases with the propagation of the fracture in the form of a power law up to a critical value. At present, the fracture propagation resistance of the rock fracture is not fully understood, and it is not known at what scale it tends to an asymptotic value. The experiment of Labuz et al. [45,110] shows that the fracture toughness of granite increases with the increase in the fracture length when the fracture length is 10–50 mm, and remains constant when the fracture length is 80–160 mm. Kobayashi et al. [111] found that the fracture toughness of tuff remains basically constant after the fracture length exceeds 85 mm. Therefore, is the rock fracture toughness constant before the fracture length reaches the order of meters? However, this is far less than the fracture toughness of larger scale fractures, such as those evaluated by hydraulic fracturing in the field and speculated in the investigation of the dike formation by magmatic intrusions. Geologists still debate whether fracture toughness is constant during the propagation of kilometers [112]. Olson [36] and Schultz et al. [108,109,113] believe that the fracture

toughness is constant during the formation of the dyke. Scholz et al. [107] believe that the rock fracture toughness is directly proportional to the square root of the fracture length (Figure 4). The hydraulic fracturing in the field shows that if the growth of the fracture height is limited or if the injection flux is increased, the bottom-hole injection pressure obtained using constant fracture toughness is gradually lower than the measured pressure with the fracture propagation. The fracture toughness increase with fracture propagation must be used. If constant fracture toughness is used to simulate the propagation of a coin-shaped fracture, the predicted bottom-hole pressure after the fracture initiation decreases monotonically with the fracture growth and tends toward the in situ stress [100,114,115]. This is inconsistent with most experimental and field results [116–121]. Only by using the fracture toughness that increases with the fracture growth can we obtain a pressure platform that is much higher than the in situ stress after the fracture initiation [122]. These seem to indicate that the rock fracture toughness still does not approach a constant value when the fracture length reaches the order of 100 m. In addition, it has been found that the fracture toughness does not change with the specimen thickness, which is different from metal materials [104,111]. Schmidt [123] believes that the apparent fracture toughness does not change with the specimen size if the maximum tensile stress yield model is used for calculating the FPZ. Therefore, we still do not fully understand the size effect of the rock fracture toughness.

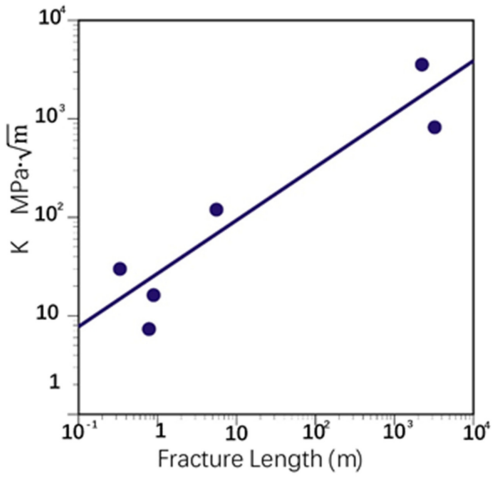


**Figure 4.** The relationship between the logarithmic median fracture length and the fracture toughness calculated using the field data on joints, veins, and dikes. Reprinted with permission from Ref. [107]. Copyright 2010, Elsevier.

Other factors may also reduce the rock apparent fracture toughness. It is found that the rock fracture toughness decreases with the increase in humidity [124–127]. The possible reason for this phenomenon is that the water reduces the surface energy of the rock and the friction resistance between grains and the fracture surface [128]. Generally, the change of the rock fracture toughness with the temperature is complicated. The experiment of Yin et al. [129] showed that when the temperature increased from 25 °C to 400 °C, the type I fracture toughness of granite decreased by 28.7%. Peng et al. [130] found that the I-type fracture toughness of granite decreased by less than 40% when the temperature increased from 20 °C to 300 °C. Funatsu et al. [102] found that the fracture toughness of Kimachi sandstone did not change significantly below 125 °C. After exceeding this temperature, the fracture toughness increases with the temperature. When the temperature reaches 200 °C, it increases by 40% compared with the value at the room temperature. When the temperature is lower than 75 °C, the fracture toughness of Tage tuff firstly decreases with an increase in the temperature, and then it increases with the temperature. When the confining pressure is added, the fracture toughness of Kimachi sandstone also increases first and then decreases with temperature. Zhang et al. [131] found that the temperature has little effect on the

dynamic fracture toughness of rocks. Therefore, the joint effect of the temperature and the confining pressure on the fracture toughness is quite complex. However, the factor of the temperature cannot explain the phenomenon that the fracture toughness under formation conditions is several orders of magnitude higher than that in the laboratory.

The rock fracture toughness under different loading modes is different. The experiment of Su et al. [132] shows that the fracture toughness of granite decreases with an increase in the mixing coefficient. There is a very good linear relationship between the fracture toughness of the pure type II and the pure type I. This was also proved by the experiment of Yin et al. [129]. For type II cracks and mixed cracks of type I and II, the fracture toughness is affected by the PFZ length and the T-stress [97,133,134]. The longer FPZ is characterized by the shear-based failure, and the shorter FPZ is characterized by the tension-based failure [133].

## 3. Fracture Process Zone

The rock FPZ size has been extensively researched by experiments and simulations. The experiment of Swanson and Spetzler [135] found that the FPZ width of Westerly granite is on the order of millimeters and the length is on the order of centimeters. The rock FPZ size obtained from different experiments is on this order of magnitude. An equation for the apparent fracture toughness related to the PFZ length was proposed by Yue et al. [91] as follows:

$$K_{\mathrm{IC}}^{\mathrm{A}} = \sqrt{\frac{8}{\pi}}\left(S\sqrt{R_f + R_c} + \sigma_T\sqrt{R_c}\right) \tag{1}$$

where $\sigma_T$ is the rock tensile strength, $R_c$ is the FPZ length, $S$ is the compressive stress, and $R_f$ is the length of the fluid lag. If the FPZ length is 10 cm, the in situ stress is 50 MPa, and the tensile strength is 1 MPa, according to this equation, the apparent fracture toughness is 25.7 MPa$\cdot\sqrt{\mathrm{m}}$. This fracture toughness is at least one order of magnitude higher than that measured in the laboratory, and is closer to the value obtained from the hydraulic fracturing practice. However, Vinegar et al. [136] found a FPZ about 14 m wide in diatomite in the South Belridge field, CA through interwell seismic and remote-well microseismic techniques. Evidence of the FPZ has been also found by other researchers in this reservoir through various seismic waves [137–140]. These results support the results of Vinegar et al. [136]. to some extent, and at least indicate that the FPZ of this reservoir is not small. The fracture half-length obtained using different methods often has a very large gap. Clarkson et al. [141] obtained a fracture half-length of about 200–300 ft from RTA, well test analysis, and fracturing simulation. The fracture half-length explained using microseismic analysis from three different vendors is about 500–700 ft. The results obtained by the RTA and well test methods are less than half of these values (Figure 5). Barree et al. [142,143] point out that the fracture half-lengths obtained from different methods are not actually the same concept. To explain the difference in the fracture half-length obtained using different methods, several fracture lengths were defined, including the microseismic length, gross created fracture length, propped length, flowing length, and effective length. Although this can qualitatively explain the difference in the fracture half-length obtained through different methods, it lacks quantitative verification. In particular, there is no quantitative explanation for the huge difference in the fracture half-length obtained through the microseismic method and other methods. It should be noted that their interpretation does not consider that the length obtained through the microseismic method includes at least part of the FPZ length, while no part of the FPZ is most likely included in the results obtained through other methods. The large length difference between them seems to indicate that the PFZ is of considerable length. We do not know why there is such a big difference between the laboratory and the field results.

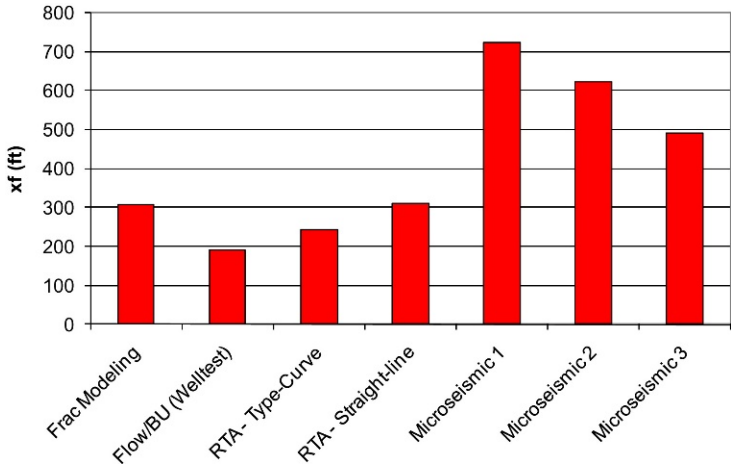


**Figure 5.** The hydraulic-fracture half-lengths ($x_f$) derived from different methods. Reprinted with permission from Ref. [141]. Copyright 2012, Elsevier.

The shape of the rock FPZ develops with the increase in the load, and generally, a strip shape is formed after reaching the peak load (Figure 6). The FPZ aspect ratio of Aue granite is 0.01–0.1 [144]. The experiment conducted by Zhang et al. [145] using sandstone shows that under peak load, the FPZ width is 0.4–0.5 times its length, and the FPZ width is significantly affected by the specimen thickness. The shape of the PFZ obtained via experiments is shown in Figure 7.

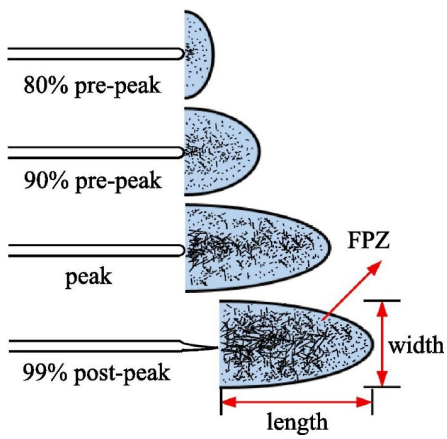


**Figure 6.** The schematic diagram of the evolution of FPZ with the increasing of load. Reprinted/adapted with permission from Ref. [145]. Copyright 2020, Elsevier.

The size and shape of the FPZ for different rocks are different. The FPZ of sandstone is shorter than that of marble [146]. The aspect ratio is affected by the rock brittleness. The more brittle the rock is, the greater the aspect ratio is [95]. The stronger the ductility of the rock, the more remarkable the size effect of the FPZ [95,96]. The simulation of Kim and Yao [147] shows that the FPZ size is affected by the rock constitutive relation and increases with the increase in the rock plasticity. The FPZ is also affected by the rock mesostructure [148,149]. The FPZ size is a function of the material grain size. It increases with the increase in the grain size [150–154]. With the increase in the grain size, the rock ductility increases [155]. Barton [148] noted that the FPZ size is 5–10 times the grain size. The FPZ size of Stockbndge dolomite is 20–40 times the grain diameter [156]. Wawersik and Brace [157] believe that the grain size affects the rock stress state, thus affecting the FPZ size. Liu et al. [158] also proved this through the simulation of the particle flow code. The simulation of Papanastasiou [27] shows that the FPZ size increases with the in situ stress deviation, and is also affected by the rock strength, Young's modulus, and pumping

parameters, while the apparent fracture toughness is directly affected by the FPZ. When the fracture propagates to a certain extent, the FPZ and the apparent fracture toughness tend to an asymptotic value. The FPZ size obtained through different methods is quite different. Zang et al. [144] found that the FPZ size obtained via acoustic emission is nine times that of the grain diameter, while that obtained through the optical crack inspection is twice that of the grain diameter.

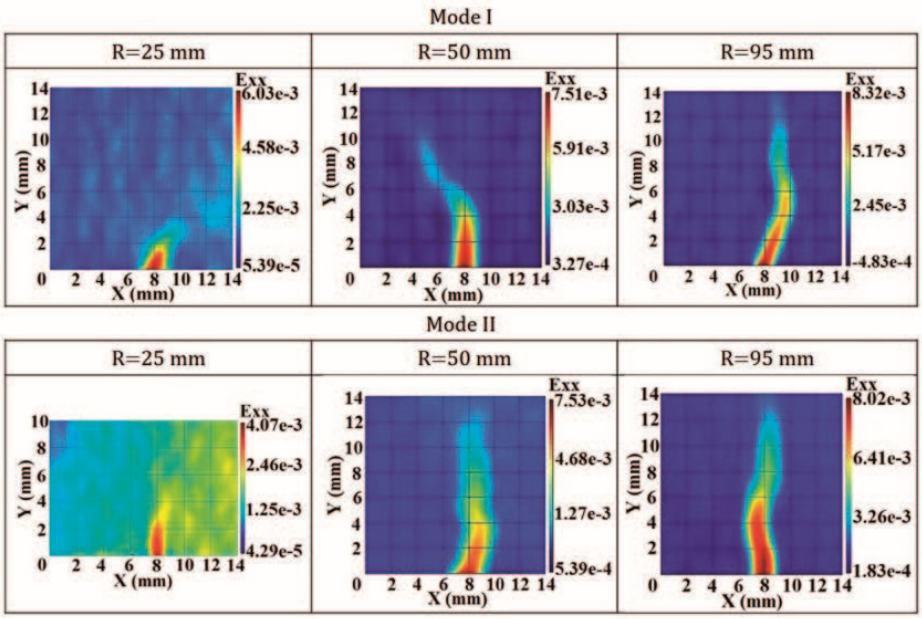


**Figure 7.** The FPZ obtained using the digital image correlation method based on horizontal strain contours in 98% of fracture load for marble SCB. Reprinted from Ref. [146]. Copyright 2019, SAGE Publications (SAGE has opted out of notification under the STM Permissions Guidelines for republication of material within the agreed-upon thresholds between STM Permissions Guidelines signatories).

The FPZ size also has a scale effect [159]. The possible reason for why the apparent fracture toughness increases with the fracture length is that the FPZ increases with the fracture length. The study of Bahrami and Mortazavi [160] shows that the FPZ size increases with the increase in the fracture length. Field observation shows that the FPZ size of the dyke is in direct proportion to the fracture size [35,161,162]. However, the experiments of Lin et al. [163] show that the FPZ length does not change with the fracture propagation.

The scale effect of the FPZ is also reflected in that the FPZ size is affected by the specimen size [164,165]. This is shown in Figure 8. In this regard, there are many contradictions in the early experimental results, which have been clearly understood in recent years. The fracture experiment conducted by Kong et al. [166] using granite shows that the FPZ width remains approximately unchanged. The experiments carried out by Chen et al. [167] with sandstone show that the length and width of the FPZ remain approximately unchanged. However, the FPZ width is slightly less than the length. This may be related to the larger size of the specimen, which is 400 mm $\times$ 400 mm $\times$ 50 mm, reaching the order of decimeters. Le et al. [168] also obtained a constant FPZ size. Zietlow and Labuz [169] found that the length and width of the FPZ changes with the specimen, but the change of the width is very small. Therefore, they believe that the FPZ width can be regarded as the material property. This is consistent with the experimental and numerical simulation results of Berea sandstone, and Berea and charcoal granite by Tarokh et al. [170]. To achieve this result, the specimen size should reach tens of centimeters. Further research has shown that the FPZ width is not constant. Numerical simulations and experiments show that there is a linear relation between the reciprocal of the width and length of the FPZ and the reciprocal of the

specimen size [94]. Based on Bazant's scaling law, the following equation was proposed by Fakhimi and Tarokh [94],

$$W = \frac{W_\infty D}{D_{\mathrm{OW}}\left(1 + \frac{D}{D_{\mathrm{OW}}}\right)} \tag{2}$$

where $W$ is the width or the length of the FPZ; $D$ is a characteristic dimension of the specimen; $D_{\mathrm{ow}}$ is a constant, and $W_\infty$ is the width or the length of the FPZ for very large specimens. The numerical simulation of Fakhimi and Wan [171,172] found that the FPZ increases with an increase in specimen size, and finally, it tends to a constant value. The width–length ratio of the FPZ remains unchanged. This means that the size effect of the FPZ disappears. However, the simulation study of Galouei and Fakhimi [95] concluded that the width–length ratio of the FPZ changed with the specimen size. The simulation results of Wan and Fakhimi [172] show that when the specimen size is less than a certain value, the FPZ size decreases with the increase in the fracture size. The reason for this phenomenon may be that the simulated specimen size is too small. Tarokh et al. [173] found that the representative element volume of the FPZ length is larger than that of the FPZ width (Figure 9). This is also proven by the simulation of Galouei and Fakhimi [95]. In addition to the specimen size, the FPZ length is also affected by the specimen shape [174].

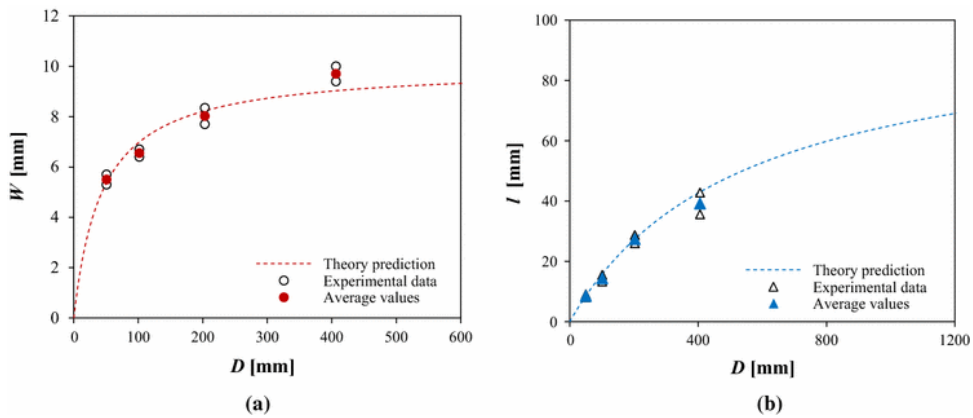


**Figure 8.** The influence of the specimen size on the FPZ size. (**a**) Width. (**b**) Length. ($W$ and $l$ are the width and length of the PFZ, respectively; $D$ is the diameter of the specimen.) Reprinted with permission from Ref. [173]. Copyright 2017, Springer Nature.

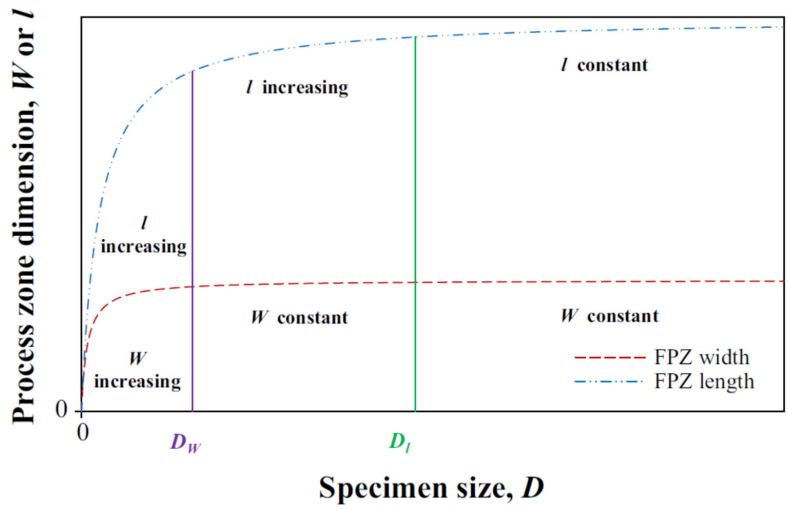


**Figure 9.** The concept map of the effect of specimen size on the dimensions of the FPZ. Reprinted with permission from Ref. [173]. Copyright 2017, Springer Nature.

The FPZ size is affected by the loading rate [175,176]. The type I–II mixed fracture experiment conducted by Xing [177] shows that the FPZ length increases from 5 mm to 17 mm with the loading rate from 0.02 to 2 mm/min. It is found that the FPZ width also increases with the fracture propagation speed [144]. Chen et al. [178] found that the FPZ not only increases with the increase in the fracture propagation speed, but also develops from semi-elliptic to strip type. This can also explain that the rock fracture toughness increases with the increase in the loading rate [179]. Under the cyclic load, more fragments are produced in the FPZ and more microcracks are formed [180].

The pore fluid also influences the size of rock FPZ. Nie et al. [181] found in the experiment that the rock FPZ is affected by the fluid in the pores. The FPZ of the water-saturated specimen is 30% longer than that of the dry specimen, and the capillary force can reduce the FPZ length. The FPZ size of the oil–water-saturated specimen is 20% smaller than that of a single-phase oil- or a single-phase water-saturated specimen.

The three-point bending mixed fracture experiment of Berea sandstone conducted by Lin and Labuz [163,182] shows that when $K_{\mathrm{II}}/K_{\mathrm{I}} < 12\%$, the FPZ is dominated by the opening displacement. The length of the FPZ increases with an increase in the mixing degree from mode I to mode II cracks [146,163]. With the increase in the specimen size, the difference of the FPZ lengths caused by the loading mode and the specimen shape become smaller and smaller [146]. Studies have shown that pure type II loading does not necessarily produce type II cracks [183–186]. Garg et al. [187] carried out the three-point bending fracture experiment using Barre granite. Although it is pure type II loading, the fracture initiates with a type I crack. If there is no confining pressure, it is difficult for the type II fracture to occur. The FPZ is dominated by tensile microcracks and a small amount of shear microcracks [175,188,189]. These may be related to the fact that the rock shear strength is much greater than its tensile strength. According to the analysis by Van Dam and Pater [190], the fracture surface roughness is related to the size of the FPZ. The fracture tip first experiences shear failure and then tensile failure. The fracture process is the combination of the tensile failure and the shear failure.

The rock fracture toughness measured in the laboratory is in the order of $O(1)$, which is often very different from the results speculated by the hydraulic fracturing in the field. Therefore, it cannot be used for a hydraulic fracturing simulation. To ensure that the $K$-control fracture is effective in the fracture toughness test, it is generally required that the fracture length and ligament length are 15–25 times of the size of the FPZ [191]. The length of the FPZ measured in the experiment often reaches the order of several centimeters to decimeters. While the FPZ size tends to the asymptotic value, it may reach the order of meters. This requires the specimen size to reach the order of meters. At present, the specimen size used in the test of the rock fracture toughness is generally in the order of centimeters to decimeters, which is far from meeting the requirements of small-scale yields. This is also an important reason for why the rock fracture toughness tested in the laboratory cannot meet the requirements of the hydraulic fracturing in the field.

## 4. Fracture Propagation Criterion for Ductile Rocks

There are two differences between the hydraulic fracturing and the linear elastic fracture theory: the fluid lag zone and the long FPZ. Garagash et al. [55] studied the applicability of the linear elastic fracture mechanics in the hydraulic fracturing. The feasibility of the linear elastic fracture mechanics depends on two parameters: the ratio of the cohesive-to-fluid-lag fracture energy, and the ratio of the cohesive-to-in situ stress. Since the formation stress is much higher than the rock cohesion, the linear elastic fracture mechanics cannot be used for the hydraulic fracturing. In the classical fracture mechanics theory, the stress intensity factor theory of the linear elastic fracture was modified by Irwin under the assumption of small-scale yield. It assumes that the material is perfectly elastic–plastic, and complies with the Mises yield criterion. For the rock fracture, the tensile stress yield criterion was proposed to modify the fracture toughness under small-scale yield. The fluid lag effect is not considered in these small-scale modifications. They also do not meet

the condition of a long FPZ at the rock fracture tip. The fracture opening displacement criterion proposed by Wells and the J-integral criterion proposed by Rice [192,193] have also been used by some researchers in the rock hydraulic fracturing. However, the J-integral is based on the hyperelastic constitutive relation, which is not in accordance with the nature of the rock FPZ, and its applicability is questionable. In addition, the fluid lag effect is not considered via the J-integral theory. Dugdale and Barenblatt [53,194,195] considered that there is a yield zone in front of the fracture tip. Therefore, they put forward the CZM. This model is widely used to study the effect of the rock plasticity on the hydraulic fracturing performance. Mokryakov [196] assumed that the yield stress in the cohesion zone is constant, and the analytical model of the fracture propagation in hydraulic fracturing is obtained. The effective fracture toughness is expressed as follows:

$$K_{\mathrm{IC}}^{eff} = P_{coh}\left[\frac{\pi}{2\arcsin\left(\frac{R}{L}\right)} - 1\right]\sqrt{\pi R} \tag{3}$$

where, $P_{coh}$ is the cohesive stress, $L$ is the total hydraulic fracture half-length, and $R$ is the real hydraulic fracture half-length. Bazant believes that the stress distribution in the FPZ for quasi-brittle materials conforms to the softening model. Therefore, Mokryakov's model can be improved. The CZM can be used to describe inelastic fracture propagation, and is the strongest propagation criterion [11,197]. However, the fluid lag effect is not considered by the CZM. In addition, how to choose the appropriate traction-separation law and parameters is worthy of further study. Based on the CZM, and considering the fluid lag effect, Rubin [90], and Khazan and Fialko [198] proposed the apparent fracture toughness model of rocks, which can well explain the law that the rock apparent fracture toughness increases with the increase in confining pressure. Yue et al. [91] discussed the applicability of the apparent fracture toughness model. The simulation results are very consistent with the results of the CZM with a fluid lag zone. The stress field near the fracture tip obtained by it is close to the results obtained using the fracture energy model and CZM. Using the fracture toughness measured at an unconfined state, the calculated stress at the crack tip under confining pressure is low. These models all assume that the length of the FPZ is constant. To consider that the rock fracture toughness may be positively correlated with the fracture length, a power law relation between the apparent fracture toughness and the fracture length is assumed by Liu et al. [199]. Zhang and Nakamaura [200] proposed a power law criterion for fracture propagation by increasing the peak separation stress in the surface separation energy. However, the effect of the rock plasticity on the hydraulic fracturing performance cannot be fully reflected by the apparent fracture toughness. The fracture is passivated by the plastic deformation at the fracture tip, which results in serious stress redistribution, making the closing pressure lower than the in situ stress [28]. The rock near the fracture wall has undergone plastic deformation, and the pore structure is changed. Therefore, the mechanical properties and permeabilities of these part rocks are also changed, and the opening of the fracture and the filtration of the fracturing fluid would be affected.

In addition to these fracture propagation models developed based on classical fracture mechanics, other types of fracture propagation models have also been proposed. Chudnovsky et al. [201,202] proposed the crack layer model, which is similar to the CZM, but obtained the development law of the crack layer through the thermodynamic theory. The continuum damage models are used to simulate hydraulic fracturing and to characterize the development of fractures through damage variables [203–207]. The effect of the rock plastic deformation on the hydraulic fracturing can be comprehensively reflected using this method. The continuous damage model was used by Valko and Economides [206,207] to fit the hydraulic fracturing data very well. However, the results of the local continuous damage model are grid-dependent. To this end, a non-local continuous damage model was proposed by Mostafa et al. [208,209]. However, the evolution law of the constitutive relation of damage variables needs to be further tested and developed in practical applications.

During the hydraulic fracturing, the rock fracturing is dominated by tension failure. The tensile failure theory was also used directly in the hydraulic fracturing simulation by Barree [210]. Whether it is appropriate to use the tensile strength measured at laboratory scale as the parameter for the hydraulic fracturing simulation under the field condition is a problem worthy of study. The rock in the hydraulic fracturing is often in a three-dimensional stress state. In addition to the tensile stress, there is also shear stress at the fracture tip. Therefore, it is necessary to determine the propagation direction of the fracture. The conventional methods for determining the propagation direction of the mixed fracture propagation include the maximum circumferential stress criterion, the strain energy density factor criterion, and the maximum energy release rate theory [211]. The crack tip elastic stress field of 2D plane under mixed loading can be written as [191]:

$$\sigma_{ij} \approx \frac{K_{\mathrm{I}}}{\sqrt{2\pi r}} f_{ij}^{\mathrm{I}}(\theta) + \frac{K_{\mathrm{II}}}{\sqrt{2\pi r}} f_{ij}^{\mathrm{II}}(\theta) + T\delta_{1i}\delta_{1j} \tag{4}$$

where $r$ and $\theta$ are polar coordinates with the origin at the crack tip; $K_{\mathrm{I}}$ and $K_{\mathrm{II}}$ are the modes I and II stress intensity factors, respectively; $T$ is the T-stress, and $f_{ij}^{\mathrm{I}}(\theta)$ and $f_{ij}^{\mathrm{II}}(\theta)$ are known functions of $\theta$. Therefore, the crack propagation path and fracture toughness are affected by the T-stress. These models are improved by considering the T-stress, and the obtained results are more consistent with experiments [212–216]. This is shown in Figure 10. In addition to these criteria, the R criterion is proposed by Khan [217], which holds that the fracture extends along the nearest direction from the fracture tip to the elastic zone. The T criterion for ductile fracture was proposed by Theocaris et al. [218–221], in which the Mises criterion is used to determine the elastic–plastic boundary. However, the calculation of the plastic zone is based on the small-scale yield correction of the linear elastic fracture mechanics. In addition to the tensile and shear failure, Gil and Roegiers [222] believe that volumetric strain should also be considered for the rock fracture propagation of underconsolidated reservoirs.

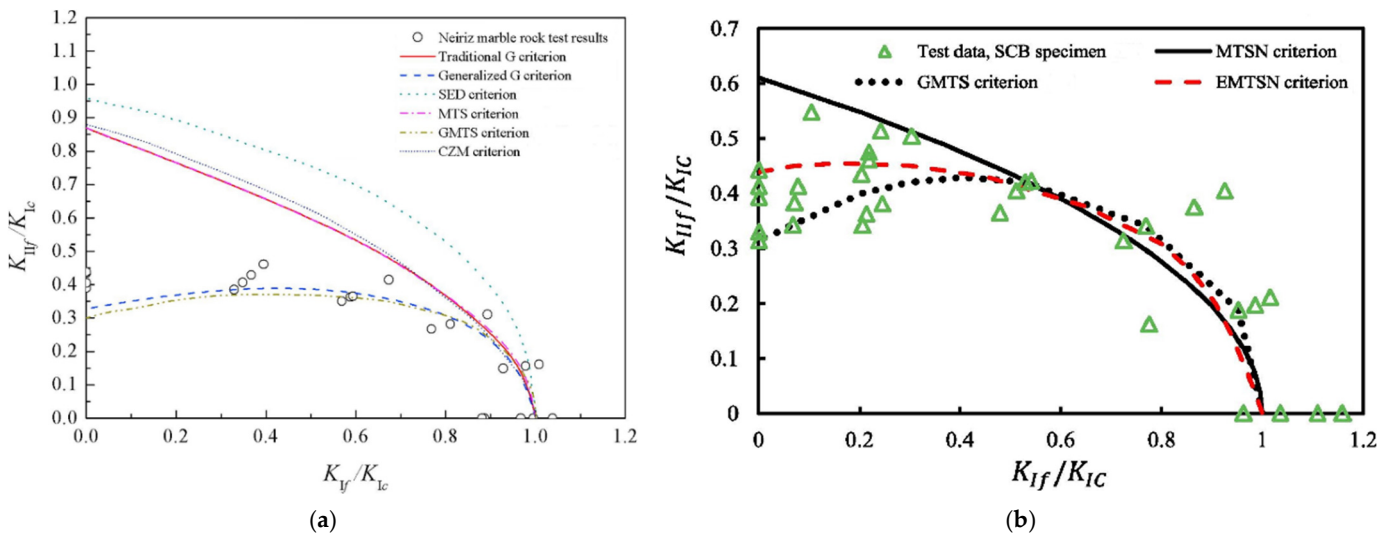


**Figure 10.** Comparisons of fracture toughness between the theoretical predictions using criteria for mixed fracture and the experimental results. (**a**) ECT specimens of Neyriz marble. Reprinted with permission from Ref. [216]. Copyright 2018, Elsevier. (**b**) SCB specimens of Neyriz and Harsin marble. Reprinted with permission from Ref. [213]. Copyright 2017, Elsevier.

## 5. Hydraulic Fracturing Simulation Method Considering Rock Plastic Deformation

There are many methods for hydraulic fracturing simulation, including the finite element method, the extended finite element method, the boundary element method/displacement discontinuity method, the discrete element method, the phase field method, and the peridynamics method, etc. For ductile rocks, the plastic deformation at the crack tip leads

to an increase in the injection fluid pressure and a change in the fracture shape. The apparent fracture toughness model, J-integral [223] and CZM model [224–229], can be used for numerical simulation, considering crack tip plasticity. In fact, these models only consider the plasticity of the zero-thickness sheet along the extension line of the crack tip. However, the plastic deformation at the crack tip has a certain thickness, and the plastic deformation also exists near the wall surface formed by the fracture propagation. In addition, the water pressure in the fracture is superimposed on the pressurized reservoir rock, which may also lead to plastic deformation of the rock near the fracture [230]. The possible nonlinear zone in the hydraulic fracturing is shown in Figure 11. The crack tip can be passivated, and the crack opening can be widened via this plastic deformation. Therefore, the geometry of the fracture is changed. Although the net pressure of the fracture propagation can be well fitted by the apparent fracture toughness model, the fracture geometry cannot be evaluated accurately [231]. Therefore, not only the crack propagation criterion considering the plastic deformation needs to be used, but also elastoplastic constitutive models characterizing the stress–strain relationship should be used to simulate the rock deformation, such as Drucker–Prager criterion [232,233], the Mohr–Coulomb criterion [234], and the Cambridge model [24,235]. Simulation results confirm that the fracture propagation pressure and fracture width are increased by the formation plasticity, and these also cause the fracture closure pressure to be lower than the minimum horizontal stress [236].

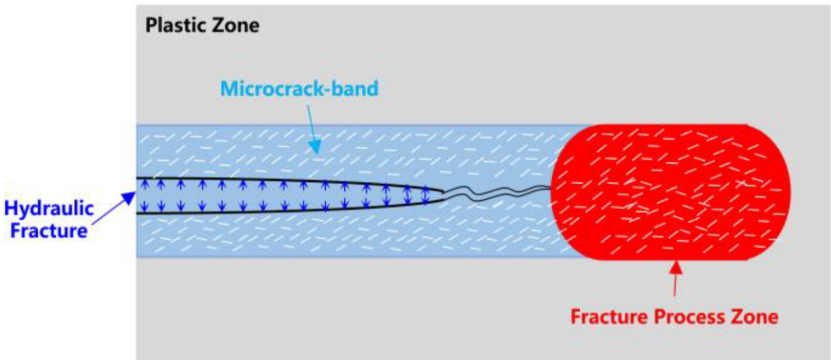


**Figure 11.** The schematic diagram of nonlinear zones caused by the hydraulic fracturing. Reprinted from Ref. [230].

At present, only a type I fracture is considered by the apparent fracture toughness models, and the CZM model is only applicable to the pre-specified propagation path. By using the global CZM model [237], the propagation path can be determined according to the propagation criterion (Figure 12). In this way, the interaction between the hydraulic fracturing fracture and the natural fracture network can be simulated [238,239]. However, the fracture propagation path is only limited to the grid boundary through this method. In order not to impose artificial restrictions on the propagation path of fractures, the XFEM is often used in simulation [240–242]. The enrichment function at the crack tip is added to the interpolation function of the FEM by the XFEM, which allows the fracture to pass through the element without re-meshing. Therefore, the non-planar propagation of fractures [243] and the mutual interference between fractures [244,245] can be simulated, and the simulation of multi-stage hydraulic fracturing is realized [246]. Further, the influence of flow in the reservoir on the hydraulic fracturing can be considered through the Biot model on the formation seepage and the pore elasticity [232]. Studies have shown that the fracture opening is reduced by the pore elasticity [236]. If the pore pressure is reduced by the generation of adjacent wells, the fractures propagation path is deflected toward the adjacent wells [247]. The shape of the plastic zone obtained by different simulation methods is inconsistent and is not always consistent with the FPZ obtained through the experiment (Figures 13 and 14).

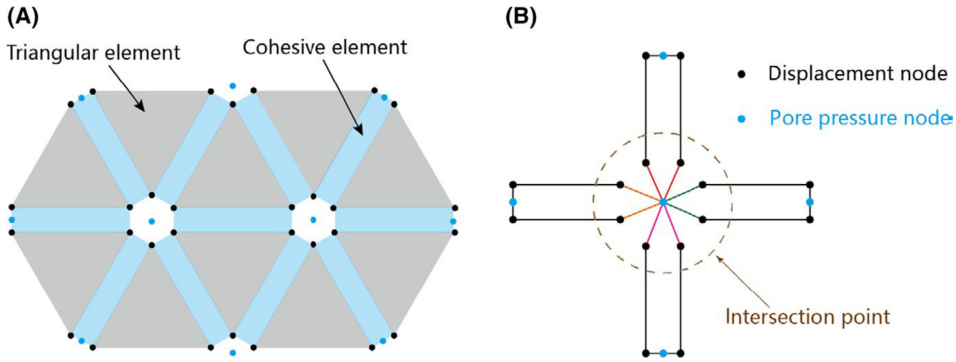


**Figure 12.** The schematic of the discretization and elements for CZM. (**A**) The mesh discretization for CZM. (**B**) The connectivity of cohesive elements. Reprinted from Ref. [238].

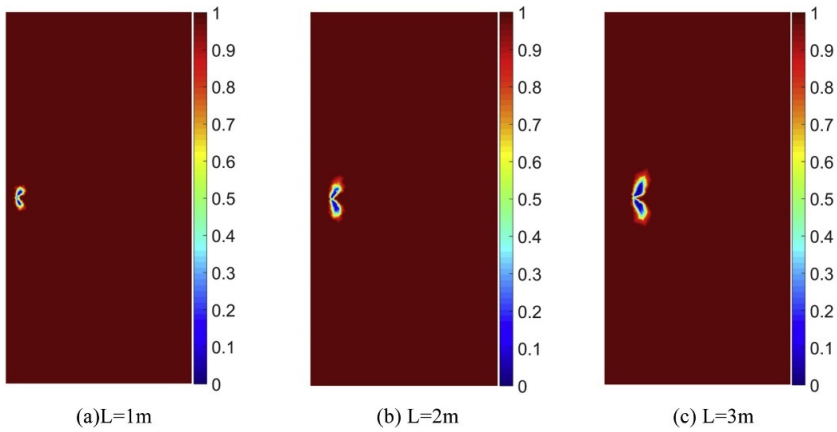


**Figure 13.** The plastic zone simulated by CZM with Drucker–Prager yield criterion. Reprinted with permission from Ref. [233]. Copyright 2018, Elsevier.

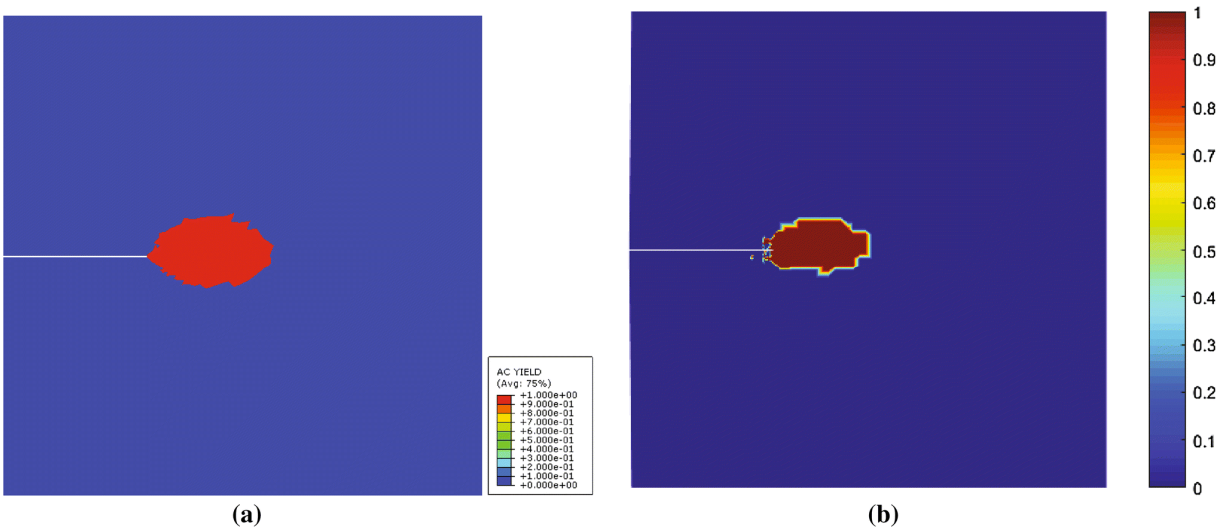


**Figure 14.** The comparison of plastic zone simulated using two methods. (**a**) Abaqus result. (**b**) XFEM result. Reprinted with permission from Ref. [223]. Copyright 2019, Springer Nature.

The CZM with fluid lag requires a very fine mesh at the fracture tip, which makes computation difficult [248]. Due to the great difference between the fluid pressure gradient in the fracture and that in the formation, the mesh around the fracture is required to be relatively dense when simulating the flow in the reservoir. This problem can be addressed by embedding discrete fractures [232,249].

In addition to these methods, the elastoplastic damage models can be used to simulate the hydraulic fracturing of ductile rocks [250,251]. Busetti et al. [252,253] used an elastoplastic continuous damage model to simulate the hydraulic fracturing process. Although the fracture propagation behavior of ductile rocks can be well simulated through this method, the width and length of the fracture cannot be revealed from this method. In addition, the fracture structure of this method depends heavily on the mesh size. Because fracture characteristics are expressed using damage variables, and the fracture characteristics is diffused over discrete areas (Figure 15), this affects the design of the proppant, fracturing fluids, and pumping procedures.

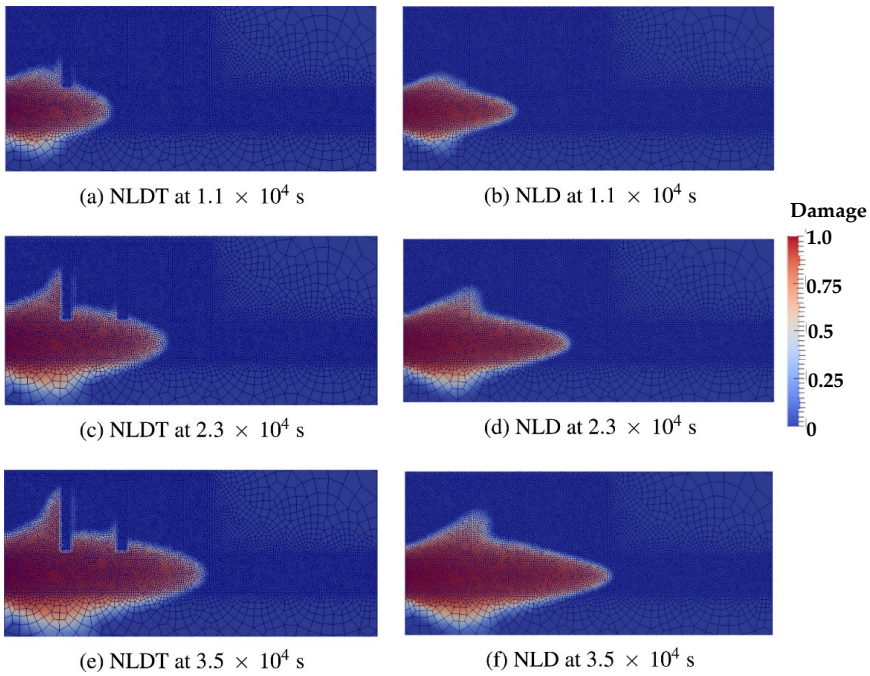


**Figure 15.** The fracture propagation characterized by the damage evolution (NLDT: non-local damage, non-local permeability; NLD: non-local damage, local permeability). Reprinted with permission from Ref. [251]. Copyright 2018, Elsevier.

## 6. Conclusions and Prospects

The fracture propagation pressure of hydraulic fracturing in ductile reservoirs is much higher than the numerical simulation results, and the rock fracture toughness estimated in the field is generally 1–3 orders of magnitude higher than the laboratory test results. It is found that the rock fracture toughness increases with the increase in the confining pressure. In addition to the energy dissipation caused by fluid viscosity and the increase in apparent fracture toughness caused by fluid lag, the FPZ at the fracture tip is the main reason for why the rock apparent fracture toughness obtained from the hydraulic fracturing in the field is much larger than that obtained through laboratory tests. The existence of FPZ can also explain the phenomenon that the rock apparent fracture toughness increases with confining pressures. The fracture tip is passivated by the FPZ, which increases the fracture propagation resistance and makes the hydraulic fracturing of ductile reservoirs more difficult. It requires higher injection pressure and results in wider and shorter fractures.

The rock FPZ size obtained from laboratory experiments is in the order of centimeters to decimeters, which is very different from the results speculated from field practice. The rock FPZ increases with an increase in the specimen size, in which the width increases faster, and the length and width tend to be constant. The FPZ size is affected by rock properties, grain size, pore fluid, temperature, loading rate, and loading configuration. Both the CZM and apparent fracture toughness model can well address the difference of the fracture toughness obtained between in the field and through the laboratory test. They

can also explain the phenomenon where the fracture toughness increases with the confining pressure. However, the CZM cannot consider the fluid lag effect. These models cannot fully consider the influence of the rock plastic deformation on the fracture propagation. At present, the CZM is mostly used in the hydraulic fracturing simulation. In order to fully consider the influence of rock plastic deformation, it is also necessary to use the elastic–plastic constitutive relation. In addition, the fluid lag and FPZ require fine grids near the crack tip, which affects the computational efficiency.

At present, there are still many unclear aspects about the fracture behavior of ductile rocks, and the difference between the fracture behavior in the hydraulic fracturing practice and the laboratory test results cannot be fully explained. The relation between the fracture toughness and fracture length at the field scale is still unclear. The rock FPZ size obtained from a hydraulic fracturing site and the laboratory is very different. In the future, it is necessary to further verify the FPZ size in reservoirs. More on-site monitoring and testing needs to be implemented for observing rock fracture behavior under different reservoir conditions. However, in hydraulic fracturing practice, the fracture may be curved. Therefore, more research is needed on the rock fracture behavior of type II and mixed type. After addressing the difference between the field and the laboratory results, it is necessary to further establish the fracture propagation criteria suitable for hydraulic fracturing simulation in ductile reservoirs.

**Author Contributions:** Conceptualization, D.Z., G.H., H.Z., M.C. and C.L.; formal analysis, D.Z., G.H. and H.Z.; investigation, D.Z., G.H. and M.C.; writing—original draft preparation, D.Z. and G.H.; writing—review and editing, G.H., H.Z., C.L. and F.Y.; visualization, D.Z.; supervision, M.C. and F.Y.; funding acquisition, G.H. All authors have read and agreed to the published version of the manuscript.

**Funding:** This research was funded by Beijing Natural Science Foundation, grant number 3212027; CNPC "Fourteenth Five Year Plan" science and technology projects, grant number 2021DJ3405.

**Data Availability Statement:** Not applicable.

**Conflicts of Interest:** The authors declare no conflict of interest.

## References

1. King, G.E. Thirty Years of Gas Shale Fracturing: What Have We Learned? In Proceedings of the SPE Annual Technical Conference and Exhibition, Florence, Italy, 19–22 September 2010.
2. Feng, Q.; Xu, S.; Xing, X.; Zhang, W.; Wang, S. Advances and challenges in shale oil development: A critical review. *Adv. Geo-Energy Res.* **2020**, *4*, 406–418. [CrossRef]
3. Han, G.; Liu, Y.; Nawnit, K.; Zhou, Y. Discussion on seepage governing equations for low permeability reservoirs with a threshold pressure gradient. *Adv. Geo-Energy Res.* **2018**, *2*, 245–259. [CrossRef]
4. Zhao, J.; Ren, L.; Jiang, T.; Hu, D.; Wu, L.; Wu, J.; Yin, C.; Li, Y.; Hu, Y.; Lin, R.; et al. Ten years of gas shale fracturing in China: Review and prospect. *Nat. Gas Ind. B* **2022**, *9*, 158–175. [CrossRef]
5. Wu, Z.; Cui, C.; Jia, P.; Wang, Z.; Sui, Y. Advances and challenges in hydraulic fracturing of tight reservoirs: A critical review. *Energy Geosci.* **2021**, *3*, 427–435. [CrossRef]
6. Li, Q.; Xing, H.; Liu, J.; Liu, X. A review on hydraulic fracturing of unconventional reservoir. *Petroleum* **2015**, *1*, 8–15. [CrossRef]
7. Wang, W.; Zheng, D.; Sheng, G.; Zhang, Q.; Su, Y. A review of stimulated reservoir volume characterization for multiple fractured horizontal well in unconventional reservoirs. *Adv. Geo-Energy Res.* **2017**, *1*, 54–63. [CrossRef]
8. Chen, B.; Barboza, B.R.; Sun, Y.; Bai, J.; Thomas, H.R.; Dutko, M.; Cottrell, M.; Li, C. A Review of Hydraulic Fracturing Simulation. *Arch. Comput. Methods Eng.* **2022**, *29*, 1–58. [CrossRef]
9. Sone, H.; Zoback, M.D. Visco-plastic properties of shale gas reservoir rocks. In Proceedings of the 45th U.S. Rock Mechanics/Geomechanics Symposium, San Francisco, CA, USA, 26–29 June 2011.
10. Martin, A.N. Crack tip plasticity: A different approach to modelling fracture propagation in soft formations. In Proceedings of the 2000 SPE Annual Technical Conference and Exhibition, Dallas, TX, USA, 1–4 October 2000.
11. Marsden, H.; Basu, S.; Striolo, A.; MacGregor, M. Advances of nanotechnologies for hydraulic fracturing of coal seam gas reservoirs: Potential applications and some limitations in Australia. *Int. J. Coal. Sci. Technol.* **2022**, *9*, 27. [CrossRef]
12. Papanastasiou, P. The influence of plasticity in hydraulic fracturing. *Int. J. Fract.* **1997**, *84*, 61–79. [CrossRef]
13. Pak, A. Numerical Modeling of Hydraulic Fracturing. Ph.D. Thesis, The University of Alberta, Edmonton, AB, Canada, 1997.
14. Jin, X.; Shah, S.N.; Sheng, M. Hydraulic fracturing model based on nonlinear fracture mechanics: Theory and simulation. In Proceedings of the SPE Annual Technical Conference and Exhibition, San Antonio, TX, USA, 8–10 October 2012.

15. Carrier, B.; Granet, S. Numerical modeling of hydraulic fracture problem in permeable medium using cohesive zone model. *Eng. Fract. Mech.* **2012**, *79*, 312–328. [CrossRef]
16. Sarris, E.; Papanastasiou, P. The influence of the cohesive process zone in hydraulic fracturing modelling. *Int. J. Fract.* **2011**, *167*, 33–45. [CrossRef]
17. Sarris, E.; Papanastasiou, P. Modeling of hydraulic fracturing in a poroelastic cohesive formation. *Int. J. Geomech.* **2012**, *12*, 160–167. [CrossRef]
18. Yao, Y.; Liu, L.; Keer, L.M. Pore pressure cohesive zone modeling of hydraulic fracture in quasi-brittle rocks. *Mech. Mater.* **2015**, *83*, 17–29. [CrossRef]
19. Wang, Y.; Fotios, K. Induced stresses near a hydraulic fracture and fracture geometry with plasticity. In Proceedings of the SPE Asia Pacific Hydraulic Fracturing Conference, Beijing, China, 24–26 August 2016.
20. Cleary, M.P.; Wright, C.A.; Wright, T.B. Experimental and modeling evidence for major changes in hydraulic fracturing design and field procedures. In Proceedings of the SPE Gas Technology Symposium, Houston, TX, USA, 22 January 1991.
21. Papanastasiou, P.; Thiercelin, M. Influence of inelastic rock behaviour in hydraulic fracturing. *Int. J. Rock Mech. Min. Sci. Geomech. Abstr.* **1993**, *30*, 1241–1247. [CrossRef]
22. Papanastasiou, P.; Atkinson, C. Representation of crack-tip plasticity in pressure sensitive geomaterials: Large scale yielding. *Int. J. Fract.* **2006**, *139*, 137–144. [CrossRef]
23. Sarris, E.; Papanastasiou, P. Numerical modeling of fluid-driven fractures in cohesive poroelastoplastic continuum. *Int. J. Numer. Anal. Meth. Geomech.* **2013**, *37*, 1822–1846. [CrossRef]
24. Zaki, K.S.; Wang, G.; Meng, F.; Abou-Sayed, A.S. A 3-D plastic fracture simulation to assess fracture volumes in compacting reservoir. In Proceedings of the Gulf Rocks 2004, the 6th North America Rock Mechanics Symposium (NARMS): Rock Mechanics Across Borders and Disciplines, Houston, TX, USA, 5–9 June 2004.
25. Parker, M.; Petre, E.; Dreher, D.; Buller, D. Haynesville shale: Hydraulic fracture stimulation approach. In Proceedings of the International Coalbed & Shale Gas Symposium, Tuscaloosa, AL, USA, 18–22 May 2009.
26. Germanovich, L.N.; Astakhov, D.K.; Shlyapobersky, J.; Mayerhofer, M.J.; Dupont, C.; Ring, L.M. Modeling multi-segmented hydraulic fracture in two extreme cases: No leak-off and dominating leak-off. *Int. J. Rock Mech. Min. Sci.* **1998**, *35*, 551–554. [CrossRef]
27. Papanastasiou, P. The effective fracture toughness in hydraulic fracturing. *Int. J. Fract.* **1999**, *96*, 127–147. [CrossRef]
28. Van Dam, D.B.; Papanastasiou, P.; De Pater, C.J. Impact of rock plasticity on hydraulic fracture propagation and closure. *SPE Prod. Facil.* **2002**, *17*, 149–159. [CrossRef]
29. Medlin, W.L.; Fitch, J.L. Abnormal treating pressures in MHF treatments. In Proceedings of the 58th SPE Annual Technical Conference, San Francisco, CA, USA, 5 October 1983.
30. Shlyapobersky, J.; Chudnovsky, A. Review of recent developments in fracture mechanics with petroleum engineering applications. In Proceedings of the SPE/ISRM Rock Mechanics in Petroleum Engineering Conference, Delft, The Netherlands, 29 August 1994.
31. Shlyapobersky, J.; Issa, M.A.; Issa, M.A.; Islam, M.; Dudley, J.W.; Shulkin, Y.; Chudnovsky, A. Scale effects on fracture growth resistance in poroelastic materials. In Proceedings of the SPE Annual Technical Conference and Exhibition, Orleans, LA, USA, 27 September 1998.
32. Shlyapobersky, J. Energy analysis of hydraulic fracturing. In Proceedings of the 26th US Symposium on Rock Mechanics (USRMS), Rapid City, SD, USA, 26 June 1985.
33. Shlyapobersky, J.; Wong, G.; Walhaug, W. Overpressure calibrated design of hydraulic fracture stimulations. In Proceedings of the SPE Annual Technical Conference and Exhibition, Houston, TX, USA, 2 October 1988.
34. Bunger, A.P. A rigorous tool for evaluating the importance of viscous dissipation in sill formation: It's in the tip. *Geol. Soc. Lond. Spec. Publ.* **2008**, *304*, 71–81. [CrossRef]
35. Rivalta, E.; Taisne, B.; Bunger, A.; Katz, R. A review of mechanical models of dike propagation: Schools of thought, results and future directions. *Tectonophysics* **2015**, *638*, 1–42. [CrossRef]
36. Olson, J.E. Sublinear scaling of fracture aperture versus length: An exception or the rule? *J. Geophys. Res. Solid Earth* **2003**, *108*, 2413. [CrossRef]
37. Delaney, P.T.; Pollard, D.D. *Deformation of Host Rocks and Flow of Magma during Growth of Minette Dikes and Breccia-Bearing Intrusions Near Ship Rock, New Mexico*; Geological Survey Professional Paper 1202; United States Government Printing Office: Washington, DC, USA, 1981.
38. Jin, Z.H.; Johnson, S.E. Magma-driven multiple dike propagation and fracture toughness of crustal rocks. *J. Geophys. Res. Solid Earth* **2008**, *113*, B03206. [CrossRef]
39. Rivalta, E.; Dahm, T. Acceleration of buoyancy-driven fractures and magmatic dikes beneath the free surface. *Geophys. J. Int.* **2006**, *166*, 1424–1439. [CrossRef]
40. Bunger, A.; Cruden, A. Modeling the growth of laccoliths and large mafic sills: Role of magma body forces. *J. Geophys. Res.* **2011**, *116*, B02203. [CrossRef]
41. Atkinson, B.K. Subcritical crack growth in geological materials. *J. Geophys. Res. Solid Earth* **1984**, *89*, 4077–4114. [CrossRef]
42. Atkinson, B.K.; Meredith, P.G. Experimental fracture mechanics data for rocks and minerals. In *Fracture Mechanics of Rock*; Atkinson, B.K., Ed.; Academic Press: London, UK, 1987; pp. 477–525.
43. Palmer, I.D.; Veatch, R.W., Jr. Abnormally high fracturing pressures in step-rate tests. *SPE Prod. Eng.* **1990**, *5*, 315–323. [CrossRef]

44. Bunger, A.; Lecampion, B. Four critical issues for successful hydraulic fracturing applications. In *Rock Mechanics and Engineering, Vol. 5: Surface and Underground Projects*; Feng, X., Ed.; CRC Press: London, UK, 2017; pp. 551–593.
45. Labuz, J.; Shah, S.; Dowding, C. Experimental analysis of crack propagation in granite. *Int. J. Rock Mech. Min. Sci. Geomech. Abstr.* **1985**, *22*, 85–98. [CrossRef]
46. Garagash, D.I. Roughness-dominated hydraulic fracture propagation. In Proceedings of the 2015 AGU Fall Meeting Abstracts, AGU, San Francisco, CA, USA, 17 December 2015.
47. Warpinski, N.R. Measurement of width and pressure in a propagating hydraulic fracture. *Soc. Petrol. Eng. J.* **1985**, *25*, 46–54. [CrossRef]
48. Bunger, A.P.; Detournay, E.; Jeffrey, R.G. Crack tip behavior in near-surface fluid-driven fracture experiments. *Comptes Rendus Mécanique* **2005**, *333*, 299–304. [CrossRef]
49. Groenenboom, J.; Dam, D.V. Monitoring hydraulic fracture growth: Laboratory experiments. *Geophysics* **2000**, *65*, 603–611. [CrossRef]
50. Ispas, I.; Eve, R.; Hickman, R.J.; Keck, R.G.; Willson, S.M.; Olson, K.E. Laboratory testing and numerical modelling of fracture propagation from deviated wells in poorly consolidated formations. In Proceedings of the SPE Annual Technical Conference and Exhibition, San Antonio, TX, USA, 8 October 2012.
51. Naidu, R.N.; Rylance, M. A simple method for identifying fracture initiation pressure. In Proceedings of the SPE/IADC Drilling Conference and Exhibition, The Hague, The Netherlands, 14 March 2017.
52. Van Dam, D.B. The Influence of Inelastic Rock Behaviour on Hydraulic Fracture Geometry. Ph.D. Thesis, Delft University of Technology, Delft, The Netherlands, 1999.
53. Barenblatt, G.I. The mathematical theory of equilibrium cracks in brittle fracture. *Adv. Appl. Mech.* **1962**, *7*, 55–129.
54. Bazant, Z.P.; Le, J.L. *Probabilistic Mechanics of Quasibrittle Structures*; Cambridge University Press: Cambridge, UK, 2017.
55. Garagash, D.I. Cohesive-zone effects in hydraulic fracture propagation. *J. Mech. Phys. Solids* **2019**, *133*, 103727. [CrossRef]
56. Swanson, P.L. Tensile fracture resistance mechanisms in brittle polycrystals: An ultrasonics and in situ microscopy investigation. *J. Geophys. Res.* **1987**, *92*, 8015–8036. [CrossRef]
57. Johnson, E.; Cleary, M.P. Implications of recent laboratory experimental results for hydraulic fractures. In Proceedings of the Low Permeability Reservoir Symposium, Denver, CO, USA, 15 April 1991.
58. Moradian, Z.; Fathi, A.; Evans, B. Shear reactivation of natural fractures in hydraulic fracturing. In Proceedings of the 50th US Rock Mechanics/Geomechanics Symposium, Houston, TX, USA, 26–29 June 2016.
59. Rahman, M.; Hossain, M.; Rahman, S. A shear-dilation-based model for evaluation of hydraulically stimulated naturally fractured reservoirs. *Int. J. Numer. Anal. Methods Geomech.* **2002**, *26*, 469–497. [CrossRef]
60. Zoback, M.D.; Kohli, A.; Das, I.; Mcclure, M.W. The importance of slow slip on faults during hydraulic fracturing stimulation of shale gas reservoirs. In Proceedings of the SPE Americas Unconventional Resources Conference, Pittsburgh, PA, USA, 5 June 2012.
61. Feng, R.; Sarmadivaleh, M. Shear dilation in hydraulic fracturing: Insight from Laboratory experiment. In Proceedings of the 53rd US Rock Mechanics/Geomechanics Symposium, New York, NY, USA, 23–26 June 2019.
62. Abou-Sayed, A.S.; Brechtel, C.E.; Clifton, R.J. In situ stress determination by hydrofracturing: A fracture mechanics approach. *J. Geophys. Res.* **1978**, *83*, 2851. [CrossRef]
63. Ito, T.; Evans, K.; Kawai, K.; Hayashi, K. Hydraulic fracture reopening pressure and the estimation of maximum horizontal stress. *Int. J. Rock Mech. Min. Sci.* **1999**, *36*, 811–826. [CrossRef]
64. Lhomme, T.; Detournay, E.; Jeffrey, R.G. Effect of fluid compressibility and borehole on the initiation and propagation of a tranverse hydraulic fracture. *Strength Fract. Complex.* **2005**, *3*, 149–162.
65. Lakirouhani, A.; Detournay, E.; Bunger, A. A reassessment of in situ stress determination by hydraulic fracturing. *Geophys. J. Int.* **2016**, *205*, 1859–1873. [CrossRef]
66. Gao, Y.; Detournay, E. Fracture toughness interpretation from breakdown pressure. *Eng. Fract. Mech.* **2021**, *243*, 107518. [CrossRef]
67. Gao, Y.; Eve, R.; Heller, R.; Ispas, I.; McLennan, J.; Detournay, E. A reinterpretation of fracture toughness from fluid injection testing. In Proceedings of the 55th US Rock Mechanics/Geomechanics Symposium, Houston, TX, USA, 21–25 June 2021.
68. Mahrer, K.D. Microseismic logging: A new hydraulic fracture diagnostic method. In Proceedings of the 1991 SPE Joint Rocky Mountain Regional/Low Permeability Reservoirs Symposium, Denver, CO, USA, 15–17 April 1991.
69. Mahrer, K.D.; Mauk, F.J. Seismic wave motion for a new model of hydraulic fracture with an induced low-velocity zone. *J. Geophys. Res.* **1987**, *92*, 9293–9309. [CrossRef]
70. Warpinski, N.R.; Teufel, L.W. Influence of geologic discontinuities on hydraulic fracture propagation. *J. Pet. Technol.* **1987**, *39*, 209–220. [CrossRef]
71. Warpinski, N.R.; Lorenz, J.C.; Branagan, P.T.; Myal, F.R.; Gall, B.L. Examination of a cored hydraulic fracture in a deep gas well. *SPE Prod. Fac.* **1993**, *8*, 150–158. [CrossRef]
72. Delaney PTPollard, D.D.; Ziony, J.I.; McKee, E.H. Field relations between dikes and joints: Emplacement processes and paleostress analysis. *J. Geophys. Res. Solid Earth* **1986**, *91*, 4920–4938. [CrossRef]
73. Perkins, T.K.; Krech, W.W. Effect of cleavage rate and stress level on apparent surface energies of rocks. *Soc. Petrol. Eng. J.* **1966**, *6*, 308–314. [CrossRef]
74. Thiercelin, M. Fracture toughness under confining pressure using the modified ting test. In Proceedings of the 28th U.S. Symposium on Rock Mechanics (USRMS), Tucson, AZ, USA, 29 June 1987.

75. Al-Shayea, N.A.; Khan, K.; Abduljauwad, S.N. Effects of confining pressure and temperature on mixed-mode (I–II) fracture toughness of a limestone rock. *Int. J. Rock Mech. Min. Sci.* **2000**, *37*, 629–643. [CrossRef]
76. Guo, H.; Aziz, N.I.; Schmidt, L.C. Rock fracture-toughness determination by the Brazilian Test. *Eng. Geol.* **1993**, *33*, 177–188. [CrossRef]
77. Schmidt, R.; Huddle, C. Effect of confining pressure on fracture toughness of Indiana limestone. *Int. J. Rock Mech. Min. Sci. Geomech. Abstr.* **1977**, *14*, 289–293. [CrossRef]
78. Gehne, S.; Forbes Inskip, N.D.; Benson, P.M.; Meredith, P.G.; Koor, N. Fluid-driven tensile fracture and fracture toughness in Nash point shale at elevated pressure. *J. Geophys. Res. Solid Earth* **2020**, *125*, 1–11. [CrossRef]
79. Stanchits, S.; Burghardt, J.; Surdi, A. Hydraulic fracturing of heterogeneous rock monitored by acoustic emission. *Rock Mech. Rock Eng.* **2015**, *48*, 2513–2527. [CrossRef]
80. Stoeckhert, F.; Brenne, S.; Molenda, M.; Alber, M. Mode I fracture toughness of rock under confining pressure. In Proceedings of the ISRM International Symposium—EUROCK 2016, Ürgüp, Turkey, 29 August 2016.
81. Chandler, M.R.; Mecklenburgh, J.; Rutter, E.; Lee, P. Fluid injection experiments in shale at elevated confining pressures: Determination of flaw sizes from mechanical experiments. *J. Geophys. Res. Solid Earth* **2019**, *124*, 5500–5520. [CrossRef]
82. Thallak, S.; Holder, J.; Gray, K. The pressure dependence of apparent hydrofracture toughness. In Proceedings of the 34th US Symposium on Rock Mechanics (USRMS), Madison, WI, USA, 28 June 1993.
83. Bohloli, B.; de Pater, C.J. Experimental study on hydraulic fracturing of soft rocks: Influence of fluid rheology and confining stress. *J. Pet. Sci. Eng.* **2006**, *53*, 1–12. [CrossRef]
84. Omori, Y.; Jin, S.; Ito, T.; Nagano, Y.; Sekine, K. Experimental study of hydraulic fracturing in unconsolidated sands using X-ray CT method. In Proceedings of the 47th U.S. Rock Mechanics/Geomechanics Symposium, San Francisco, CA, USA, 23 June 2013.
85. De Pater, C.J.; Dong, Y.; Bohloli, B. Experimental study of hydraulic fracturing in sand as a function of stress and fluid rheology. In Proceedings of the SPE Hydraulic Fracturing Technology Conference, College Station, TX, USA, 29 January 2007.
86. Germanovich, L.N.; Hurt, R.S.; Ayoub, J.A.; Siebrits, E.; Norman, D.; Ispas, I.; Montgomery, C.T. Experimental study of hydraulic fracturing in unconsolidated materials. In Proceedings of the SPE International Symposium and Exhibition on Formation Damage Control, Lafayette, LA, USA, 15 February 2012.
87. Golovin, E.; Jasarevic, H.; Chudnovsky, A.; Dudley, J.W.; Wong, G.K. Observation and Characterization of Hydraulic Fracture in Cohesionless Sand. In Proceedings of the 44th U.S. Rock Mechanics Symposium and 5th U.S.-Canada Rock Mechanics Symposium, Salt Lake City, UT, USA, 27 June 2010.
88. Brooks, Z.; Ulm, F.J.; Einstein, H.H.; Abousleiman, Y. A nanomechanical investigation of the crack tip process zone. In Proceedings of the 44th US Rock Mechanics Symposium and 5th U.S.-Canada Rock Mechanics Symposium, Salt Lake City, UT, USA, 27–30 June 2010.
89. Hashida, T.; Oghikubo, H.; Takahashi, H.; Shoji, T. Numerical simulation with experimental verification of the fracture behavior in granite under confining pressures based on the tension-softening model. *Int. J. Fract.* **1993**, *59*, 227–244. [CrossRef]
90. Rubin, A.M. Tensile fracture of rock at high confining pressure: Implications for dike propagation. *J. Geophys. Res. Solid Earth* **1993**, *98*, 15919–15935. [CrossRef]
91. Yue, K.; Lee, H.P.; Olson, J.E.; Schultz, R.A. Apparent fracture toughness for LEFM applications in hydraulic fracture modeling. *Eng. Fract. Mech.* **2020**, *230*, 106984. [CrossRef]
92. Rocco, C.; Guinea, G.V.; Planas, J.; Elices, M. Size effect and boundary conditions in the Brazilian test: Experimental verification. *Mater. Struct.* **1999**, *32*, 210–217. [CrossRef]
93. Ayatollahi, M.R.; Akbardoost, J. Size and geometry effects on rock fracture toughness: Mode I fracture. *Rock Mech. Rock Eng.* **2014**, *47*, 677–687. [CrossRef]
94. Fakhimi, A.; Tarokh, A. Process zone and size effect in fracture testing of rock. *Int. J. Rock Mech. Min. Sci.* **2013**, *60*, 95–102. [CrossRef]
95. Galouei, M.; Fakhimi, A. Size effect, material ductility and shape of fracture process zone in quasi-brittle materials. *Comput. Geotech.* **2015**, *65*, 126–135. [CrossRef]
96. Fakhimi, A.; Galouei, M. Size effect on length and width of fracture process zone. In Proceedings of the 49th US Rock Mechanics/Geomechanics Symposium, San Francisco, CA, USA, 28 June–1 July 2015.
97. Aliha, M.R.M.; Ayatollahi, M.R.; Smith, D.J.; Pavier, M.J. Geometry and size effects on fracture trajectory in a limestone rock under mixed mode loading. *Eng. Fract. Mech.* **2010**, *77*, 2200–2212. [CrossRef]
98. Bazant, Z.P.; Gettu, R.; Kazemi, M.T. Identification of nonlinear fracture properties from size effect tests and structural analysis based on geometry-dependent R-curves. *Int. J. Rock Mech. Min. Sci.* **1991**, *28*, 43–51. [CrossRef]
99. Khan, K.; Al-Shayea, N.A. Effect of specimen geometry and testing method on mixed mode I–II fracture toughness of a limestone rock from Saudi Arabia. *Rock Mech. Rock Eng.* **2000**, *33*, 179–206. [CrossRef]
100. Wei, M.D.; Dai, F.; Xu, N.W.; Zhao, T.; Xia, K.W. Experimental and numerical study on the fracture process zone and fracture toughness determination for ISRM-suggested semicircular bend rock specimen. *Eng. Fract. Mech.* **2016**, *154*, 43–56. [CrossRef]
101. Funatsu, T.; Shimizu, N.; Kuruppu, M.; Matsui, K. Evaluation of mode I fracture toughness assisted by the numerical determination of K-resistance. *Rock Mech. Rock Eng.* **2015**, *48*, 143–157. [CrossRef]
102. Funatsu, T.; Seto, M.; Shimada, H.; Matsui, K.; Kuruppu, M. Combined effects of increasing temperature and confining pressure on the fracture toughness of clay bearing rocks. *Int. J. Rock Mech. Min. Sci.* **2004**, *41*, 927–938. [CrossRef]

103. Ingraffea, A.R.; Schmidt, R.A. Experimental verification of a fracture mechanics model for tensile strength prediction of Indiana limestone. In Proceedings of the 19th U.S. Symposium on Rock Mechanics (USRMS), Reno, NV, USA, 1 May 1978.
104. Schmidt, R.A.; Lutz, T.J. $K_{Ic}$ and $J_{Ic}$ of Westerly granite—Effects of thickness and in-plane dimensions. In Proceedings of the 11th Symposium on Fracture Mechanics, Blacksburg, VA, USA, 12 June 1978.
105. Hashida, T.; Sato, K.; Takahashi, H. Significance of crack opening for determining the growth behavior monitoring of hydrofractures. In Proceedings of the Eighteenth Workshop on Geothermal Reservoir Engineering, Stanford, CA, USA, 26–28 January 1993; pp. 79–84.
106. Weisinger, R.; Costin, L.S.; Lutz, T.J. $K_{Ic}$ and J-resistance-curve measurements on Nevada Tuff. *Exp. Mech.* **1980**, *26*, 68–72. [CrossRef]
107. Scholz, C.H. A note on the scaling relations for opening mode fractures in rock. *J. Struct. Geol.* **2010**, *32*, 1485–1487. [CrossRef]
108. Schultz, R.A.; Soliva, R.; Fossen, H.; Okubo, C.H.; Reeves, D.M. Dependence of displacement–length scaling relations for fractures and deformation bands on the volumetric changes across them. *J. Struct. Geol.* **2008**, *30*, 1405–1411. [CrossRef]
109. Schultz, R.A.; Mège, D.; Diot, H. Emplacement conditions of igneous dikes in Ethiopian traps. *J. Volcanol. Geotherm. Res.* **2008**, *178*, 683–692. [CrossRef]
110. Labuz, J.F.; Shah, S.P.; Dowding, C.H. The fracture process zone in granite: Evidence and effect. *Int. J. Rock Mech. Min. Sci. Geomech. Abstr.* **1987**, *24*, 235–246. [CrossRef]
111. Kobayashi, R.; Matsuki, K.; Otsuka, N. Size effect in the fracture toughness in Ogina Tuff. *Int. J. Rock Mech. Min. Sci. Geomech. Abstr.* **1986**, *23*, 13–18. [CrossRef]
112. Olson, J.E.; Schultz, R.A. Comment on "A note on the scaling relations for opening mode fractures in rock" by C.H. Scholz. *J. Struct. Geol.* **2011**, *33*, 1523–1524. [CrossRef]
113. Schultz, R.A.; Klimczak, C.; Fossen, H.; Olson, J.E.; Exner, U.; Reeves, D.M.; Soliva, R. Statistical tests of scaling relationships for geologic structures. *J. Struct. Geol.* **2013**, *48*, 85–94. [CrossRef]
114. Abe, H.; Mura, T.; Keer, L.M. Growth rate of a penny-shape crack in hydraulic fracturing of rocks. *J. Geophys. Res.* **1976**, *8*, 5335–5340. [CrossRef]
115. Savitski, A.; Detournay, E. Propagation of a fluid-driven penny-shaped fracture in an impermeable rock: Asymptotic solutions. *Int. J. Solids Struct.* **2002**, *39*, 6311–6337. [CrossRef]
116. Daneshy, A.A. Hydraulic Fracture Propagation in Layered Formations. *SPE J.* **1978**, *18*, 33–41. [CrossRef]
117. Roodhart, L.P.; Fokker, P.A.; Davies, D.R.; Shlyapobersky, J.; Wong, G.K. Frac-and Pack Stimulation: Application, Design, and Field Experience. *J. Pet. Technol.* **1994**, *46*, 230–238. [CrossRef]
118. Johnson, D.E.; Wright, C.A.; Stachel, A.; Schmidt, H.; Cleary, M.P. On-site real-time analysis allows optimal propped fracture stimulation of a complex gas reservoir. In Proceedings of the SPE 25414, SPE Production Operations Symposium, Oklahoma City, OK, USA, 21–23 March 1993.
119. Chudnovsky, A.; Fan, F.; Shulkin, Y.; Dudley, J.W.; Nichols, W.B.; Wong, G.K. Hydraulic Fracture Containment in Layered Media, Experiment and Computer Simulation. In Proceedings of the 38th US Rock Mechanics Symposium, Washington, DC, USA, 10–12 June 2001.
120. Britt, L.K.; Smith, M.B.; Cunningham, L.E.; Waters, F.; Dannish, G.A.; Lachance DMackow, H.M. Frac-packing high-permeability sands in the mahogany field, offshore Trinidad. In Proceedings of the SPE Annual Technical Conference, Dallas, TX, USA, 1–4 October 2000.
121. Kizaki, A.; Ohashi, K.; Tanaka, H.; Sakaguchi, K. Effects of vertical stress on fracture propagation using super critical carbon dioxide. In *Rock Mechanics for Resources, Energy and Environment*; Kwasniewski, M., Lydzba, D., Eds.; Taylor & Francis Group: London, UK, 2013.
122. Chudnovsky, A.; Fan, F.; Shulkin, Y.; Zhang, H.; Dudley, J.W.; Wong, G.K. Hydraulic Fracture Simulation Revisited. In Proceedings of the 42nd US Rock Mechanics Symposium and 2nd U.S.-Canada Rock Mechanics Symposium, San Francisco, CA, USA, 29 June–2July 2008.
123. Schmidt, R.A. A microcrack model and its significance to hydraulic fracturing and fracture toughness testing. In Proceedings of the 21st U.S. Symposium on Rock Mechanics (USRMS), Rolla, MO, USA, 27 May 1980.
124. Haberfield, C.M.; Ian, J. Determination of fracture toughness of a saturated soft rock. *Can. Geotech. J.* **1990**, *27*, 276–284. [CrossRef]
125. Lim, I.L.; Johnston, I.W.; Choi, S.K.; Boland, J.N. Fracture testing of a soft rock with semi-circular specimens under three point bending, part 1: Mode-I. *Int. J. Rock Mech. Min. Sci. Geomech. Abstr.* **1994**, *31*, 185–197. [CrossRef]
126. Kenner, V.H.; Advani, S.H.; Richard, T.G. A Study of Fracture Toughness for an anisotropic Shale. In Proceedings of the 23rd U.S. Symposium on Rock Mechanics(USRMS), Berkeley, CA, USA, 25 August 1982; pp. 471–479.
127. Singh, R.N.; Sun, G.X. An investigation into the factors affecting the fracture toughness of coal measures sandstones. *J. Mines Met. Fuels* **1990**, *38*, 111–118.
128. Rao, K.S.; Rao, G.V.; Ramamurthy, T. A comparative evaluation of rock strength measurement: Discussion of paper by K.L. Gunsallus and F.H. Kulhawy. Int. J. Rock Mech. Min. Sci. & Geomech. Abstr. 21, 233–248 (1984). *Int. J. Rock Mech. Min. Sci. Geomech. Abstr.* **1987**, *24*, 193–196.
129. Yin, T.B.; Wu, Y.; Wang, C.; Zhuang, D.D.; Wu, B.Q. Mixed-mode I+II tensile fracture analysis of thermally treated granite using straight-through notch Brazilian disc specimens. *Eng. Fract. Mech.* **2020**, *234*, 107111. [CrossRef]
130. Peng, K.; Lv, H.; Zou, Q.; Wen, Z.; Zhang, Y. Evolutionary characteristics of mode-I fracture toughness and fracture energy in granite from different burial depths under high-temperature effect. *Eng. Fract. Mech.* **2020**, *239*, 107306. [CrossRef]

131. Zhang, Z.X.; Yu, J.; Kou, S.Q.; Lindqvist, P.-A. Effects of high temperatures on dynamic rock fracture. *Int. J. Rock Mech. Min. Sci.* **2001**, *38*, 211–225. [CrossRef]
132. Su, H.; Qin, X.; Feng, Y.; Yu, L.; Sun, Z. Experimental investigation of mixed mode I-II fracture property of thermally treated granite under dynamic loading. *Theor. Appl. Fract. Mech.* **2022**, *118*, 103267. [CrossRef]
133. Ali, A.; Bahador, B.; Reza, A.M.; Morteza, N. On the role of fracture process zone size in specifying fracturing mechanism under dominant mode II loading. *Theor. Appl. Fract. Mech.* **2022**, *117*, 103150.
134. Rashidi Moghaddam, M.; Ayatollahi, M.R.; ·Berto, F. Rock fracture toughness under mode ii loading: A theoretical model based on local strain energy density. *Rock Mech. Rock Eng.* **2018**, *51*, 243–253. [CrossRef]
135. Swanson, P.L.; Spetzler, H. Ultrasonic probing of the fracture process zone in rock using surface waves. In Proceedings of the 25th U.S. Symposium on Rock Mechanics (USRMS), Evanston, IL, USA, 25 June 1984.
136. Vinegar, H.J.; Wills, P.B.; DeMartini, D.C.; Shlyapobersky, J.; Deeg, W.F.J.; Adair, R.G.; Woerpel, J.C.; Fix, J.E.; Sorrells, G.G. Active and passive seismic imaging of a hydraulic fracture in Diatomite. *J. Pet. Technol.* **1992**, *44*, 28–90. [CrossRef]
137. Meadows, M.A.; Winterstein, D.F. Seismic detection of a hydraulic fracture from shear-wave VSP data at Lost Hills Field, California. *Geophysics* **1994**, *59*, 11–26. [CrossRef]
138. IIderton, D.C.; Patzek, T.W.; Rector, J.W.; Vinegar, H.J. Passive imaging of hydrofractures in the south Belridge Diatomite. *SPE Form. Eval.* **1996**, *11*, 46–54. [CrossRef]
139. Block, L.V.; Cheng, C.H.; Fehler, M.C.; Phillips, W.S. Seismic imaging using microearthquakes induced by hydraulic fracturing. *Geophysics* **1994**, *59*, 102–112. [CrossRef]
140. Rector, J.W., III; Dong, Q.; Patzek, T.W. Passive characterization of hydrofracture properties using signals from hydraulic pumps. *J. Pet. Sci. Eng.* **2000**, *27*, 49–58. [CrossRef]
141. Clarkson, C.R.; Jensen, J.L.; Chipperfield, S. Unconventional gas reservoir evaluation: What do we have to consider? *J. Nat. Gas Sci. Eng.* **2012**, *8*, 9–33. [CrossRef]
142. Barree, R.D.; Cox, S.A.; Gilbert, J.V.; Dobson, M. Closing the gap: Fracture half-length from design, buildup, and production analysis. *SPE Prod. Facil.* **2005**, *20*, 274–285. [CrossRef]
143. Barree, R.D.; Duenckel, R.J.; Hlidek, B.T. The Limits of Fluid Flow in Propped Fractures- the Disparity Between Effective Flowing and Created Fracture Lengths. In Proceedings of the SPE Hydraulic Fracturing Technology Conference and Exhibition, The Woodlands, TX, USA, 5–7 February 2019.
144. Zang, A.; Wagner, F.C.; Stanchits, S.; Janssen, C.; Dresen, G. Fracture process zone in Granite. *J. Geophys. Res.* **2000**, *105*, 23651–23661. [CrossRef]
145. Zhang, S.; Wang, H.; Li, X.; Zhang, X.; An, D.; Yu, B. Experimental study on development characteristics and size effect of rock fracture process zone. *Eng. Fract. Mech.* **2021**, *241*, 107377. [CrossRef]
146. Moazzami, M.; Ayatollahi, M.R.; Akhavan-Safar, A. Assessment of the fracture process zone in rocks using digital image correlation technique: The role of mode-mixity, size, geometry and material. *Int. J. Damage Mech.* **2020**, *29*, 646–666. [CrossRef]
147. Kim, K.; Yao, C. The influence of constitutive behavior on the fracture process zone and stress field evolution during hydraulic fracturing. In Proceedings of the 1st North American Rock Mechanics Symposium, Austin, TX, USA, 1 June 1994.
148. Barton, C.C. Variables in fracture energy and toughness testing of rock. In Proceedings of the 23rd U.S Symposium on Rock Mechanics (USRMS), Berkeley, CA, USA, 25 August 1982.
149. Brooks, Z.; Ulm, F.J.; Einstein, H.H. Role of microstructure size in fracture process zone development of marble. In Proceedings of the 46th U.S. Rock Mechanics/Geomechanics Symposium, Chicago, IL, USA, 24-27 June 2012.
150. Tarokh, A.; Fakhimi, A. Discrete element simulation of the effect of particle size on the size of fracture process zone in quasi-brittle materials. *Comput. Geotech.* **2014**, *62*, 51–60. [CrossRef]
151. Bochenek, A.; Prokopski, G. The investigation of aggregate grain size effect on fracture toughness of ordinary concrete structures. *Int. J. Fract.* **1989**, *41*, 197–205. [CrossRef]
152. Dempsey, J.P.; Adamson, R.M.; Mulmule, S.V. Scale effects on the in-situ tensile strength and fracture of ice. Part II: First-year sea ice at Resolute, N.W.T. *Int. J. Fract.* **1999**, *95*, 347. [CrossRef]
153. Dempsey, J.P.; Defranco, S.J.; Adamson, R.M.; Mulmule, S.V. Scale effects on the in-situ tensile strength and fracture of ice. Part I: Large grained freshwater ice at Spray Lakes Reservoir, Alberta. *Int. J. Fract.* **1999**, *95*, 325. [CrossRef]
154. Ouchterlony, F. Review of fracture toughness testing of rocks. *SM Arch.* **1982**, *7*, 131–211.
155. Tarokh, A.; Fakhimi, A. Relationship between grain size and fracture properties of rock. In Proceedings of the 47th US Rock Mechanics/Geomechanics Symposium, San Francisco, CA, USA, 23–26 June 2013.
156. Nolen-Hoeksema, R.C.; Gordon, R.B. Optical detection of crack patterns in the opening-mode fracture of Marble. *Int. J. Rock Mech. Min. Sci. Geomech. Abstr.* **1987**, *24*, 135–144. [CrossRef]
157. Wawersik, W.R.; Brace, W.F. Post-failure behavior of a granite and diabase. *Rock Mech.* **1971**, *3*, 61–85. [CrossRef]
158. Liu, H.Z.; Lin, J.-S.; He, J.-D.; Xie, H.-Q. Size effect and fracture: A discrete modeling perspective. In Proceedings of the 51st US Rock Mechanics/Geomechanics Symposium, San Francisco, CA, USA, 25–28 June 2017.
159. Bazant, Z.P.; Kazemi, M.T. Determination of fracture energy, process zone length and brittleness number from size effect, with application to rock and concrete. *Int. J. Fract.* **1990**, *44*, 111–131. [CrossRef]

160. Bahrami, V.; Mortazavi, A. A numerical investigation of hydraulic fracturing process in oil reservoirs using non-linear fracture mechanics. In Proceedings of the ISRM International Symposium—5th Asian Rock Mechanics Symposium, Tehran, Iran, 24 November 2008.
161. Pollard, D.D.; Segall, P. Theoretical displacements and stresses near fractures in rock: With applications to faults, joints, veins, dikes, and solution surfaces. In *Fracture Mechanics of Rock*; Atkinson, B.K., Ed.; Academic Press: London, UK, 1987; pp. 277–349.
162. Engvik, A.K.; Bertram, A.; Kalthoff, J.F.; Stöckhert, B.; Austrheim, H.; Elvevold, S. Magma-driven hydraulic fracturing and infiltration of fluids into the damaged host rock, an example from Dronning Maud Land, Antarctica. *J. Struct. Geol.* **2005**, *27*, 839–854. [CrossRef]
163. Lin, Q.; Yuan, H.N.; Biolzi, L.; Labuz, J.F. Opening and Mixed Mode Fracture Process in a Quasi-Brittle Material via Digital Imaging. *Eng. Fract. Mech.* **2014**, *131*, 176–193. [CrossRef]
164. Zhang, S.; Wang, L.; Gao, M. Experimental investigation of the size effect of the mode I static fracture toughness of limestone. *Adv. Civil Eng.* **2019**, *2019*, 1–11. [CrossRef]
165. Wei, M.; Dai, F.; Xu, N.; Zhao TLiu, Y. An experimental and theoretical assessment of semi-circular bend specimens with chevron and straight-through notches for mode I fracture toughness testing of rocks. *Int. J. Rock Mech. Min. Sci.* **2017**, *99*, 28–38. [CrossRef]
166. Lie, K.; Gamage, R.P.; Zhao, J.; Rathnaweera, T.; Ma, Z. Tensile behaviors of Granite: Grain scale cracking and fracture process zone. In Proceedings of the 53rd US Rock Mechanics/Geomechanics Symposium, New York, NY, USA, 23–26 June 2019.
167. Chen, L.; Zhang, G.; Zou, Z.; Guo, Y.; Du, X. Experimental observation of fracture process zone in sandstone from digital imaging. In Proceedings of the 54th US Rock Mechanics/Geomechanics Symposium, Golden, CO, USA, 28 June–1 July 2020.
168. Le, J.-L.; Manning, J.; Labuz, J.F. Scaling of fatigue crack growth in rock. *Int. J. Rock Mech. Min. Sci.* **2014**, *72*, 71–79. [CrossRef]
169. Zietlow, W.K.; Labuz, J.F. Measurement of the intrinsic process zone in rock using acoustic emission. *Int. J. Rock Mech. Min. Sci.* **1998**, *35*, 291–299. [CrossRef]
170. Tarokh, A.; Fakhim, A.; Labuz, J.F. Size of process zone in fracture testing of rock. In Proceedings of the 46th US Rock Mechanics/Geomechanics Symposium, Chicago, IL, USA, 24–27 June 2012.
171. Fakhimi, A.; Wan, F. Discrete element modeling of the process zone shape in mode I fracture at peak load and in post-peak regime. *Int. J. Rock Mech. Min. Sci.* **2016**, *85*, 119–128. [CrossRef]
172. Wan, F.; Fakhimi, A. Numerical three-point bending test of fracture process zone in post-peak deformation of rock. In Proceedings of the 50th US Rock Mechanics/Geomechanics Symposium, Houston, TX, USA, 26–29 June 2016.
173. Tarokh, A.; Makhnenko, R.Y.; Fakhimi, A.; Labuz, J.F. Scaling of the fracture process zone in rock. *Int. J. Fract.* **2017**, *204*, 191–204. [CrossRef]
174. Wong, L.N.Y.; Guo, T.Y. Microcracking behavior of two semi-circular bend specimens in mode I fracture toughness test of granite. *Eng. Fract. Mech.* **2019**, *221*, 106565. [CrossRef]
175. Backers, T.; Stanchits, S.; Dresen, G. Tensile fracture propagation and acoustic emission activity in sandstone: The effect of loading rate. *Int. J. Rock Mech. Min. Sci.* **2005**, *42*, 1094–1101. [CrossRef]
176. Bazant, Z.P.; Bai, S.-P.; Gettu, R. Fracture of rock: Effect of loading rate. *Eng. Fract. Mech.* **1993**, *45*, 393–398. [CrossRef]
177. Xing, Y.; Huang, B.; Ning, E.; Zhao, L.; Jin, F. Quasi-static loading rate effects on fracture process zone development of mixed-mode (I-II) fractures in rock-like materials. *Eng. Fract. Mech.* **2020**, *240*, 107365. [CrossRef]
178. Chen, L.; Zhang, G.; Zou, Z.; Guo, Y.; Zheng, X. The effect of fracture growth rate on fracture process zone development in quasi-brittle rock. *Eng. Fract. Mech.* **2021**, *258*, 108086. [CrossRef]
179. Ko, T.Y.; Kemeny, J. Effect of confining stress and loading rate on fracture toughness of rocks. In Proceedings of the 1st Canada–U.S. Rock Mechanics Symposium, Vancouver, BC, Canada, 27 May 2007.
180. Ghamgosar, M.; Erarslan, N. Experimental and numerical studies on development of fracture process zone (FPZ) in rocks under cyclic and static loadings. *Rock Mech. Rock Eng.* **2016**, *49*, 893–908. [CrossRef]
181. Nie, Y.; Zhao, Z.; Zhang, G.; Zhao, B.; Jiang, Y.; Wan, B.; Zhao, H. The influence of water-oil saturation on the length of fracture process zone. In Proceedings of the 52nd US Rock Mechanics/Geomechanics Symposium, Seattle, Washington, DC, USA, 17–20 June 2018.
182. Lin, Q.; Labuz, J.F. Identifying quasi-brittle facture by AE and Digital Imaging. *J. Acoust. Emiss.* **2011**, *29*, 68–77.
183. Liu, H.Z.; Lin, J.S.; He, J.-D.; Xie, H.Q. Dominant mode of planar fractures and the role of material properties. *Eng. Fract. Mech.* **2018**, *195*, 57–79. [CrossRef]
184. Ji, W.W.; Pan, P.Z.; Lin, Q.; Feng, X.T.; Du, M.P. Do disk-type specimens generate a mode II fracture without confinement? *Int. J. Rock Mech. Min. Sci.* **2016**, *87*, 48–54. [CrossRef]
185. Lin, Q.; Ji, W.W.; Pan, P.Z.; Wang, S.; Lu, Y. Comments on the mode II fracture from disk-type specimens for rock-type materials. *Eng. Fract. Mech.* **2019**, *211*, 303–320. [CrossRef]
186. Lin, Q.; Wang, S.; Pan, P.Z.; Ji, W.W.; Lu, Y. Fracture initiation under pure shear revisited: Remarks on the mode II fracture in quasi-brittle materials. *Theor. Appl. Fract. Mech.* **2020**, *109*, 102700. [CrossRef]
187. Prasoon, G.; Ahmadreza, H.; Griffiths, D.V. Investigation of fracture process zone in Barre Granite under mode II loading. In Proceedings of the 55th US Rock Mechanics/Geomechanics Symposium, Houston, TX, USA, 20–23 June 2021.
188. Li, B.Q.; Einstein, H.H. Comparison of visual and acoustic emission observations in a four point bending experiment on barre granite. *Rock Mech. Rock Eng.* **2017**, *50*, 2277–2296. [CrossRef]
189. Nasseri, M.H.B.; Mohanty, B.; Young, R.P. Fracture toughness measurements and acoustic emission activity in brittle rocks. *Pure Appl. Geophys.* **2006**, *163*, 917–945. [CrossRef]

190. Van Dam, D.B.; de Pater, C.J. Roughness of hydraulic fractures: The importance of in-situ stress and tip processes. In Proceedings of the 1999 SPE Annual Technical Conference and Exhibition, Houston, TX, USA, 3–6 October 1999.
191. Yang, W. *Macroscopic and Microscopic Fracture Mechanics*; National Defense Industry Press: Beijing, China, 1995.
192. Rice, J.R. *Mechanics of Crack Tip Deformation and Extension by Fatigue*; ASTM STP 415; American Society for Testing and Materials: West Conshohocken, PA, USA, 1967; pp. 247–311.
193. Hilton, P.D.; Hutchinson, J.W. Plastic intensity factors for cracked plates. *Eng. Fract. Mech.* **1971**, *3*, 435–451. [CrossRef]
194. Barenblatt, G.I. The formation of equilibrium cracks during brittle fracture: General ideas and hypothesis, axially symmetric cracks. *J. Appl. Math. Mech.* **1959**, *23*, 622–636. [CrossRef]
195. Dugdale, D.S. Yielding of steel sheets containing slits. *J. Mech. Phys. Solids* **1960**, *8*, 100–104. [CrossRef]
196. Mokryakov, V. Analytical solution for propagation of hydraulic fracture with Barenblatt's cohesive tip zone. *Int. J. Fract.* **2011**, *169*, 159–168. [CrossRef]
197. Lecampion, B.; Bunger, A.; Zhang, X. Numerical methods for hydraulic fracture propagation: A review of recent trends. *J. Nat. Gas Sci. Eng.* **2018**, *49*, 66–83. [CrossRef]
198. Khazan, Y.M.; Fialko, Y.A. Fracture criteria at the tip of fluid-driven cracks in the earth. *Geophys. Res. Lett.* **1995**, *22*, 2541–2544. [CrossRef]
199. Liu, D.; Lecampion, B.; Garagash, D.I. Propagation of a fluid-driven fracture with fracture length dependent apparent toughness. *Eng. Fract. Mech.* **2019**, *220*, 106616. [CrossRef]
200. Zhang, Z.; Nakamura, T. Simulations of crack propagation in elastic-plastic graded materials. *Mech. Mater.* **2004**, *36*, 601–622.
201. Chudnovsky, N. *Crack Layer Theory*; NASA Report 17463; Case Western University: Cleveland, OH, USA, 1984.
202. Chudnovsky, N.; Fan, J.; Shulkin, Y.; Dudley, J.W.; Shlyapobersky, J.; Shraufnagel, R. A new hydraulic fracture tip mechanism in a statistically homogenous medium. In Proceedings of the SPE Annual Technical Conference and Exhibition, Denver, CO, USA, 6–9 October 1996.
203. Valkó, P.; Economides, M.J. Continuum Damage Mechanics Model of Hydraulic Fracturing. *J. Pet. Technol.* **1993**, *45*, 198–205. [CrossRef]
204. Kemp, L.F. Discussion of Continuum Damage Mechanics Model of Hydraulic Fracturing. *J. Pet. Technol.* **1993**, *45*, 338.
205. Germanovich, L.N.; Roegiers, J.-C. Discussion of Continuum Damage Mechanics Model of Hydraulic Fracturing. *J. Pet. Technol.* **1993**, *45*, 1191–1193.
206. Valko, P.; Economides, M.J. Reply to Discussion of Continuum Damage Mechanics Model of Hydraulic Fracturing. *J. Pet. Technol.* **1993**, *45*, 1191. [CrossRef]
207. Valco, P.; Economides, M.J. Propagation of hydraulically induced fractures—A continuum damage mechanics approach. *Int. J. Rock Mech. Min. Sci. Geomech. Abstr.* **1994**, *31*, 221–229. [CrossRef]
208. Mobasher, M.E.; Waisman, H. Non-local continuum damage and transport modeling framework for hydraulic fracturing. In Proceedings of the ARMA/DGS/SEG International Geomechanics Symposium, Online, 1–4 November 2021.
209. Mobasher, M.E.; Waisman, H.; Woelke, P.B. A Continuum Non-Local Damage-Transport Model for Hydraulic Fracturing. In Proceedings of the 54th US Rock Mechanics/Geomechanics Symposium, Golden, CO, USA, 28 June–1 July 2020.
210. Barree, R.D. A Practical numerical simulator for three- dimensional fracture propagation in heterogeneous media. In Proceedings of the SPE Reservoir Simulation Symposium, San Francisco, CA, USA, 15–18 November 1983.
211. Li, S.; He, T.; Yin, X. *Rock Fracture Mechanics*; Science Press: Beijing, China, 2016.
212. Smith, D.J.; Ayatollahi, M.R.; Pavier, M.J. The role of T-stress in brittle fracture for linear elastic materials under mixed-mode loading. *Fatigue Fract. Eng. Mater. Struct.* **2001**, *24*, 137–150. [CrossRef]
213. Mirsayar, M.M.; Razmi, A.; Aliha, M.R.M.; Berto, F. EMTSN criterion for evaluating mixed mode I/II crack propagation in rock materials. *Eng. Fract. Mech.* **2018**, *190*, 186–197. [CrossRef]
214. Ayatollahi, M.R.; Rashidi Moghaddam, M.; Berto, F. A generalized strain energy density criterion for mixed mode fracture analysis in brittle and quasi-brittle materials. *Theor. Appl. Fract. Mech.* **2015**, *79*, 70–76. [CrossRef]
215. Rashidi Moghaddam, M.; Ayatollahi, M.R.; Berto, F. Mixed mode fracture analysis using generalized averaged strain energy density criterion for linear elastic materials. *Int. J. Solids Struct.* **2017**, *120*, 137–145. [CrossRef]
216. Hou, C.; Jin, X.; Fan, X.; Xu, R.; Wang, Z. A generalized maximum energy release rate criterion for mixed mode fracture analysis of brittle and quasi-brittle materials. *Theor. Appl. Fract. Mech.* **2019**, *100*, 78–85. [CrossRef]
217. Khan, S.M.A.; Khraisheh, M.K. A new criterion for mixed mode fracture initiation bases on the crack tip plastic core region. *Int. J. Plast.* **2004**, *20*, 55–84. [CrossRef]
218. Theocaris, P.S. Discussion of 'On the use of the T-criterion in fracture mechanics' by N. A. B. Yehia. *Eng. Fract. Mech.* **1986**, *24*, 371–382. [CrossRef]
219. Theocaris, P.S.; Andrianopoulos, N.P. The Mises elastic plastic boundary as the core region in fracture criteria. *Eng. Fract. Mech.* **1982**, *16*, 425–432. [CrossRef]
220. Theocaris, P.S.; Andrianopoulos, N.P. The T-criterion applied to ductile fracture. *Int. J. Fract.* **1982**, *20*, R125–R130. [CrossRef]
221. Theocaris, P.S.; Kardomateas, G.A.; Andrianopoulos, N.P. Experimental study of the T- criterion in ductile fracture. *Eng. Fracture Mech.* **1982**, *17*, 439–447. [CrossRef]
222. Gil, I.; Roegiers, J.-C. Coupled elasto-plastic model for hydraulic fracturing of unconsolidated formations. In Proceedings of the 10th ISRM Congress, Sandton, South Africa, 8 September 2003.

223. Zeng, Q.; Yao, J.; Shao, J. Effect of plastic deformation on hydraulic fracturing with extended element method. *Acta Geotech.* **2019**, *14*, 2083–2101. [CrossRef]
224. Yao, Y. Linear elastic and cohesive fracture analysis to model hydraulic fracture in brittle and ductile rocks. *Rock Mech. Rock Eng.* **2012**, *45*, 375–387. [CrossRef]
225. Manchanda, R.; Bryant, E.C.; Bhardwaj, P.; Cardiff, P.; Sharma, M.M. Strategies for effective stimulation of multiple perforation clusters in horizontal wells. *SPE Prod. Oper.* **2017**, *33*, 539–556.
226. Guo, J.; Luo, B.; Lu, C.; Lai, J.; Ren, J. Numerical investigation of hydraulic fracture propagation in a layered reservoir using the cohesive zone method. *Eng. Fract. Mech.* **2017**, *186*, 195–207. [CrossRef]
227. Dahi Taleghani, A.; Gonzalez-Chavez, M.; Yu, H.; Asala, H. Numerical simulation of hydraulic fracture propagation in naturally fractured formations using the cohesive zone model. *J. Pet. Sci. Eng.* **2018**, *165*, 42–57. [CrossRef]
228. Baykin, A.N.; Golovin, S.V. Application of the fully coupled planar 3d poroelastic hydraulic fracturing model to the analysis of the permeability contrast impact on fracture propagation. *Rock Mech. Rock Eng.* **2018**, *51*, 3205–3217. [CrossRef]
229. Zhang, G.M.; Liu, H.; Zhang, J.; Wu, H.A.; Wang, X.X. Three-dimensional finite element simulation and parametric study for horizontal well hydraulic fracture. *J. Pet. Sci. Eng.* **2010**, *72*, 310–317. [CrossRef]
230. Xing, Y.; Zhang, G.; Huang, B. Recent Advances in Nonlinear Fracturing Characteristics of the Hydraulic Fracture in the Deep Reservoir. *IOP Conf. Ser. Earth Environ. Sci.* **2020**, *570*, 032062. [CrossRef]
231. Wang, H.; Economides, M.J. Poroelastic versus poroplastic modeling of hydraulic fracturing. In Proceedings of the SPE Hydraulic Fracturing Technology Conference, The Woodlands, TX, USA, 4–6 February 2014.
232. Liu, W.; Yao, J.; Zeng, Q. A numerical hybrid model for non-planar hydraulic fracture propagation in ductile formations. *J. Pet. Sci. Eng.* **2021**, *196*, 107796. [CrossRef]
233. Liu, W.; Zeng, Q.; Yao, J. Numerical simulation of elasto-plastic hydraulic fracture propagation in deep reservoir coupled with temperature field. *J. Petrol. Sci. Eng.* **2018**, *171*, 115–126. [CrossRef]
234. Hu, Y.; Zhao, J.; Cao, L.; Zhao, J.; Li, J.; Wu, Z.; Hou, J. Numerical simulation for fracture propagation in elastoplastic formations. *Geofluids* **2021**, *2021*, 6680023. [CrossRef]
235. Lin, H.; Deng, J.G.; Liu, W.; Xie, T.; Xu, J.; Liu, H.L. Numerical simulation of hydraulic fracture propagation in weakly consolidated sandstone reservoirs. *J. Cent. South Univ.* **2018**, *25*, 2944–2952. [CrossRef]
236. Wang, H.Y.; Marongiu-Porcu, M.; Economides, M.J. Poroelastic and poroplastic modeling of hydraulic fracturing in brittle and ductile formations. *SPE Prod. Oper.* **2016**, *31*, 47–59. [CrossRef]
237. Wang, H.Y. Hydraulic fracture propagation in naturally fractured reservoirs: Complex fracture or fracture networks. *J. Nat. Gas Sci. Eng.* **2019**, *68*, 102911. [CrossRef]
238. Li, Y.; Liu, W.; Deng, J.; Yang, Y.; Zhu, H. A 2D explicit numerical scheme–based pore pressure cohesive zone model for simulating hydraulic fracture propagation in naturally fractured formation. *Energy Sci. Eng.* **2019**, *7*, 1527–1543. [CrossRef]
239. Sun, T.; Zeng, Q.; Xing, H. A quantitative model to predict hydraulic fracture propagating across cemented natural fracture. *J. Pet. Sci. Eng.* **2022**, *208*, 109595. [CrossRef]
240. Mohammadnejad, T.; Khoei, A. An extended finite element method for hydraulic fracture propagation in deformable porous media with the cohesive crack model. *Finite Elem. Anal. Des.* **2013**, *73*, 77–95. [CrossRef]
241. Mohammadnejad, T.; Khoei, A. Hydro-mechanical modeling of cohesive crack propagation in multiphase porous media using the extended finite element method. *Int. J. Numer. Anal. Methods Geo Mech.* **2013**, *37*, 1247–1279. [CrossRef]
242. Liu, F.; Gordon, P.; Meier, H.; Valiveti, D. A stabilized extended finite element framework for hydraulic fracturing simulations. *Int. J. Numer. Anal. Methods GeoMech.* **2017**, *41*, 654–681. [CrossRef]
243. Wang, H.Y. Numerical modeling of non-planar hydraulic fracture propagation in brittle and ductile rocks using XFEM with cohesive zone method. *J. Pet. Sci. Eng.* **2015**, *135*, 127–140. [CrossRef]
244. Paul, B.; Faivre, M.; Massin, P.; Giot, R.; Colombo, D.; Golfier, F.; Martin, A. 3D coupled HM–XFEM modeling with cohesive zone model and applications to non planar hydraulic fracture propagation and multiple hydraulic fractures interference. *Comput. Methods Appl. Mech. Eng.* **2018**, *342*, 321–353. [CrossRef]
245. Liu, F.; Gordon, P.A.; Valiveti, D.M. Modeling competing hydraulic fracture propagation with the extended finite element method. *Acta Geotech.* **2018**, *13*, 243–265. [CrossRef]
246. Wang, H.Y. Numerical investigation of fracture spacing and sequencing effects on multiple hydraulic fracture interference and coalescence in brittle and ductile reservoir rocks. *Eng. Fract. Mech.* **2016**, *157*, 107–124. [CrossRef]
247. Wang, H. Poro-elasto-plastic modeling of complex hydraulic fracture propagation: Simultaneous multi-fracturing and producing well interference. *Acta Mech.* **2016**, *227*, 507–525. [CrossRef]
248. Liu, D.; Lecampion, B. Propagation of a plane-strain hydraulic fracture accounting for the presence of a cohesive zone and a fluid lag. In Proceedings of the 53rd US Rock Mechanics/Geomechanics Symposium, New York, NY, USA, 23–26 June 2019.
249. Liu, W.; Zeng, Q.; Yao, J.; Liu, Z.; Li, T.; Yan, X. Numerical study of elasto-plastic hydraulic fracture propagation in deep reservoirs using a hybrid EDFM–XFEM method. *Energies* **2021**, *14*, 2610. [CrossRef]
250. Shojaei, A.; Dahi Taleghani, A.; Li, G. A continuum damage failure model for hydraulic fracturing of porous rocks. *Int. J. Plast.* **2014**, *59*, 199–212. [CrossRef]
251. Mobasher, M.E.; Waisman, H.; Berger-Vergiat, L. Thermodynamic framework for non-local transport-damage modeling of fluid driven fracture in porous media. *Int. J. Rock Mech. Min. Sci.* **2018**, *111*, 64–83. [CrossRef]

252. Busetti, S.; Mish, K.; Reches, Z. Damage and plastic deformation of reservoir rocks: Part 1. Damage fracturing. *AAPG Bull.* **2012**, *96*, 1687–1709. [CrossRef]
253. Busetti, S.; Mish, K.; Hennings, P.; Reches, Z. Damage and plastic deformation of reservoir rocks: Part 2. Propagation of a hydraulic fracture. *AAPG Bull.* **2012**, *96*, 1711–1732. [CrossRef]